

H₂S scavenger as a broad-spectrum strategy to deplete bacteria-derived H₂S for antibacterial sensitization

Received: 12 June 2024

Accepted: 18 October 2024

Published online: 31 October 2024



Jiekai Sun^{1,4}, Xu Wang^{1,4}, Ye Gao^{1,4}, Shuangyu Li^{1,4}, Ziwei Hu¹, Yan Huang¹, Baoqiang Fan², Xia Wang¹, Miao Liu¹, Chunhua Qiao¹, Wei Zhang^{1,2}✉, Yipeng Wang^{1,3}✉ & Xingyue Ji¹✉

Bacteria-derived H₂S plays multifunctional protective roles against antibiotics insult, and the H₂S biogenesis pathway is emerging as a viable target for the antibacterial adjuvant design. However, the development of a pan-inhibitor against H₂S-synthesizing enzymes is challenging and underdeveloped. Herein, we propose an alternative strategy to downregulate the H₂S levels in H₂S-producing bacteria, which depletes the bacteria-derived H₂S chemically by H₂S scavengers without acting on the synthesizing enzymes. After the screening of chemically diversified scaffolds and a structural optimization campaign, a potent and specific H₂S scavenger is successfully identified, which displays efficient H₂S depletion in several H₂S-producing bacteria, potentiates both bactericidal agents and photodynamic therapy, enhances the bacterial clearance of macrophages and polymorphonuclear neutrophils, disrupts the formation of bacterial biofilm and increases the sensitivity of bacterial persister cells to antibiotics. Most importantly, such an H₂S scavenger exhibits sensitizing effects with gentamicin in *Pseudomonas aeruginosa*-infected pneumonia and skin wound female mouse models. In aggregate, our results not only provide an effective strategy to deplete bacteria-derived H₂S and establish the H₂S biogenesis pathway as a viable target for persisters and drug-resistant bacteria, but also deliver a promising antibacterial adjuvant for potential clinical translation.

The rapid and persistent emergence of drug-resistant bacteria poses a serious threat to public healthcare worldwide. In 2019, antimicrobial resistance directly led to 1.27 million deaths, which was much bigger than the number of deaths caused by HIV or malaria¹. The situation is further exacerbated by a significantly dwindling number of new antimicrobials receiving FDA approval in the past 50 years². Resistance to antibiotics is normally developed by direct mutations to the bacterial genome, which is known as genotypic resistance and results in

reduced porin protein expression, elevated expression of efflux pumps and metabolizing enzymes, or reduced binding affinity of the antibiotics toward their targets³. Besides the development of new antibiotics with novel mechanisms to combat drug resistance^{4–10}, an alternative and effective strategy is to devise antibacterial adjuvants, which by themselves display no or minimum antibacterial effects, while significantly potentiating existing antibiotics. Over the past decades, a series of such adjuvants have been elegantly developed for

¹Jiangsu Province Engineering Research Center of Precision Diagnostics and Therapeutics Development, College of Pharmaceutical Science, Soochow University, Suzhou, Jiangsu, China. ²State Key Laboratory of Microbial Technology, Shandong University, Qingdao, Shandong, China. ³Yantai Institute of Coastal Zone Research, Chinese Academy of Sciences, Yantai, China. ⁴These authors contributed equally: Jiekai Sun, Xu Wang, Ye Gao, Shuangyu Li.

✉ e-mail: zhang_wei@sdu.edu.cn; yipengwang@suda.edu.cn; jixy@suda.edu.cn

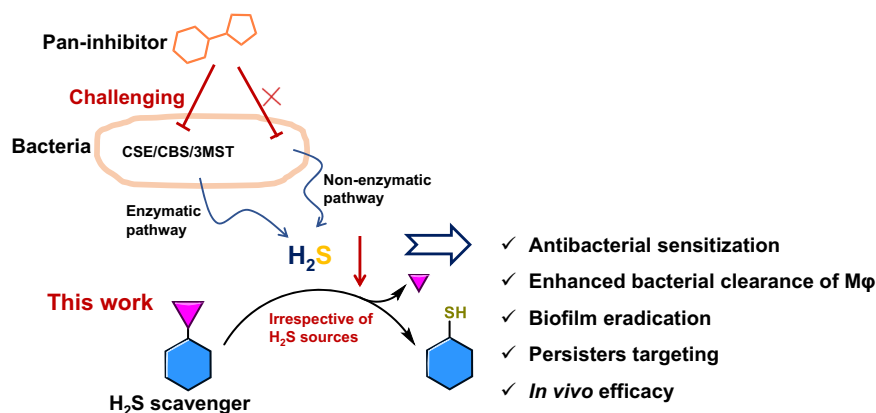


Fig. 1 | Downregulation of bacteria-derived H₂S for antibacterial sensitization and biofilm eradication via H₂S-synthesizing enzymes inhibition (previous strategy) or H₂S scavenger (this work). CSE cystathionine γ-lyase, CBS cystathionine β-synthetase, 3MST 3-mercaptopyruvate sulfurtransferase.

antibacterial sensitization and/or drug resistance reversion^{11–20}. In addition to the genotypic resistance, the bacteria can become refractory to antibiotics without genetic mutations by transiently entering dormancy, which is known as phenotypic resistance or tolerance²¹. The subpopulation of bacteria with such a phenotypic resistance is termed persisters, which reside mainly inside the biofilm, making the antibiotic effects compromised²². The persister is the main reason responsible for the failure of treatment and the relapse of drug-sensitive bacterial infections in the clinic²³. Phenotypic resistance is much more frequently observed as compared to genotypic resistance, and mounting evidence indicates that phenotypic resistance or persisters predispose to the occurrence and spread of genotypic resistance^{24–26}. Therefore, eradication of the persisters is a very promising strategy to cut off the emergence of genotypic resistance. However, despite the importance of persisters, little is known about the signaling pathways contributing to the formation of persisters, and thus no treatment is yet available in the clinic targeting the persisters^{27,28}.

Hydrogen sulfide (H₂S) is an important gasotransmitter in mammals akin to NO and CO²⁹. Recently, bacteria-derived H₂S has been demonstrated to be a universal protective reagent against antibiotic insult via its well-established antioxidant effects³⁰. The pioneering work by the Nudler group shows that H₂S is a vital contributing factor to the formation of bacterial biofilm, and the persister cells exhibited a much higher level of H₂S than the active cells. Importantly, inhibition of H₂S biogenesis significantly sensitizes bacteria and persisters to bactericidal agents both in vitro and in vivo, establishing that the H₂S biogenesis pathway is a promising target for persisters³¹. However, the development of potent H₂S biogenesis inhibitors is challenging and severely underdeveloped. Like its mammalian counterpart, there are also three H₂S-synthesizing enzymes in bacterial cells, namely cystathionine γ-lyase (CSE), cystathionine β-synthetase (CBS), and 3-mercaptopyruvate sulfurtransferase (3-MST), and different strain of bacteria relies on different enzyme for H₂S production. Although several inhibitors against these three enzymes are available³², they suffer from a low potency and/or inferior physiochemical properties, and thus high concentrations (i.e., 1 mM) are normally required to efficiently suppress H₂S synthesis in vitro³⁰. Recently, the Nudler group successfully developed a specific drug-like bacterial CSE inhibitor with IC₅₀ in the low micromolar range³¹. Such an inhibitor can sensitize *Staphylococcus aureus* and *Pseudomonas aeruginosa* to most of the bactericidal agents both in vitro and in vivo and represents a promising starting point for further development.

Different strains of bacteria rely on different enzymes to produce H₂S. For example, *P. aeruginosa* and *S. aureus* mainly employ CSE to synthesize H₂S³¹, while *E. coli*³⁰ and *V. cholerae*³³ utilize 3MST and CBS

for H₂S production, respectively. Therefore, it is highly desirable to devise a pan-inhibitor against these H₂S synthesizing enzymes for general antibacterial sensitization. However, the development of such pan-inhibitors represents an exceedingly challenging task³¹. In addition, there might exist pathways for the non-enzymatic generation of H₂S in bacteria³⁴, for which enzyme inhibitors show no effects.

In this work, we come up with an alternative strategy to deplete bacteria-derived H₂S for antibacterial sensitization. Instead of devising pan-inhibitors against the enzymes, we decide to directly eliminate the end product H₂S by a specific scavenger (Fig. 1). As such, the H₂S levels in all H₂S-producing bacteria can be readily downregulated regardless of the source of H₂S. Along this line, we identify nitrobenzofurazan scaffold for H₂S scavenger design after screening chemically diversified scaffolds. A detailed structure-activity relationships campaign leads to the identification of several potent H₂S scavengers, which exhibit efficient H₂S depletion in several H₂S-producing bacteria. One representative H₂S scavenger efficiently sensitizes *S. aureus*, *P. aeruginosa*, *E. coli*, and methicillin-resistant *S. aureus* (MRSA) to bactericidal agents and photodynamic therapy, enhances the bacterial clearance of macrophages and polymorphonuclear neutrophils (PMNs), displays the capacity to inhibit and eradicate bacterial biofilm formation, and sensitizes the persister cells to the antibiotic gentamicin (Gm). Most importantly, the representative scavenger also significantly potentiates GM in *P. aeruginosa*-infected pneumonia and skin-wound female mouse models.

Results

Identification of the hit scavenger

To identify an efficient scavenger for bacteria-derived H₂S, a methylene blue (MB) assay³⁵ was employed to screen a series of chemically diversified scaffolds, which were known to be reactive with H₂S under physiological conditions and have been extensively employed for reaction-based H₂S fluorescent probe design^{36–43}. To better distinguish the scavenging activity of different compounds, the scavenging half-lives were calculated based on the H₂S decay curves (Fig. 2C, D). Noteworthy, due to its volatile nature, H₂S concentrations in the control group also decreased along with time with a half-life of 25 min, and the addition of a potent scavenger was expected to significantly lower the decay half-life. As shown in Fig. 2C, D, two chemotypes of compounds (**3–4**, **7a**) were identified to efficiently deplete H₂S in the MB assay, in particular compounds **3** and **4**, which made H₂S undetectable just 2 min post mixing. Compounds **1–2** and **5** also exhibited some H₂S scavenging activity, but the potency was not as pronounced as those of **3–4** and **7a**. To validate these results in bacteria, compounds **3**, **4**, and **7a** were then subjected to H₂S depletion in *S. aureus* (one strain of the so-called ESKAPE bacteria) using a well-established lead

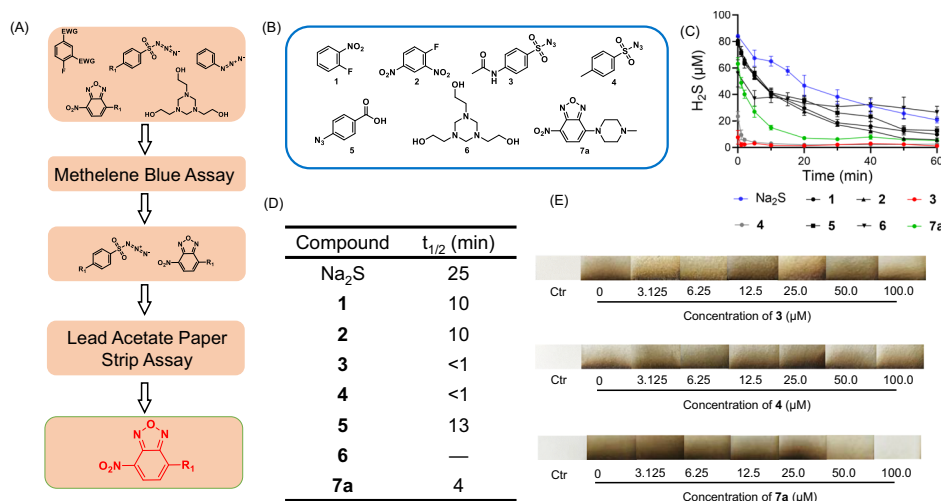


Fig. 2 | The two-step screening cascade identified a specific H₂S scavenger.

A The illustration of the screening process. **B** The chemical structures of the screened compounds. **C** H₂S (Na₂S, 100 μ M) decay curves in the presence/absence of H₂S scavengers (110 μ M) in PBS buffer (pH = 7.4) at 25 °C. The results are expressed as mean \pm S.D. n = 3 independent experiments. **D** The decay half-lives of

H₂S in the presence of the tested compounds in PBS buffer (pH = 7.4) at 25 °C. **E** The lead acetate paper strip assay indicated the H₂S depletion effects of the tested compounds in *S. aureus*. Ctr refers to the control group without the bacteria. One-way ANOVA followed by Tukey's post hoc analysis. Source data are provided as a Source Data file.

acetate paper strip assay^{30,44} As shown in Fig. 2E, *S. aureus* produced quite a lot of H₂S as indicated by the dark brown strip. Although compounds **3** and **4** could efficiently eliminate H₂S in the MB assay, they failed to do the same in *S. aureus*, presumably attributed to their unspecific reactivity toward other biothiol species. Indeed, compound **3** can be efficiently reduced in the presence of 1 mM GSH (Supplementary Fig. 10). Satisfyingly, compound **7a** dose-dependently eliminated H₂S in *S. aureus*, with complete H₂S depletion at 100 μ M.

The structural optimizations and SAR studies

To obtain more efficient H₂S scavengers and gain insights into the structure of H₂S-depletion activity relationships (SAR), we conducted a detailed structural modification toward the scaffold of compound **7a**. The reaction between H₂S and compound **7a** is a classic nucleophilic aromatic substitution reaction (Supplementary Fig. 8)⁴⁵, so the presence of the strong electron-withdrawing nitro group is indispensable for H₂S depletion. Therefore, the modifications were primarily made toward the leaving group as well as the heterocyclic rings, and a series of potential H₂S scavengers were synthesized accordingly (Supplementary Figs. 1–7). With these compounds in hand, we tested their H₂S-depletion capacity in vitro using the MB assay and calculated the H₂S decay half-lives. As shown in Table 1, several analogs displayed comparable and even better H₂S-depletion capacity than the hit compound **7a**, in particular **7b**, **7c**, **9a**, **9b**, and **9d**. Based on these results, a preliminary SAR can be concluded. As for the leaving group, replacing the N-methylpiperazine with other alkylamino (**7e**, **7f**) or phenylamino (**7d**) groups led to decreased scavenging efficiency, and the modifications at the “N” of piperazine (**7b**, **7c**) were mostly well-tolerated. However, acylation of the “N” of piperazine (**7g**) resulted in decreased activity. Altogether, these results indicated that a positive charge group at the side chain was favorable for H₂S depletion. However, compound **7j** displayed relatively weak activity, albeit with a positive charge group at the side chain, suggesting that the positive charge group with a rigid structure was beneficial for H₂S depletion. Compared with the alkylamino group, the phenoxy group is a better-leaving group, and thus compound **7i** displayed better activity as compared with **7e** and **7f**, but its activity was still inferior to that of **7a**. Such results further reiterated the importance of the rigid positive charge center for H₂S depletion. The modifications toward the heterocyclic rings were less tolerated. Replacing the oxygen atom with

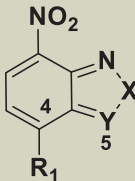
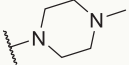
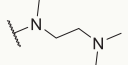
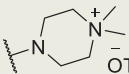
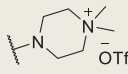
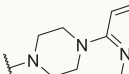
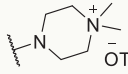
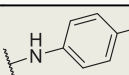
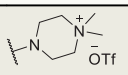
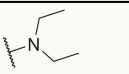
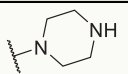
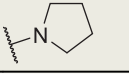
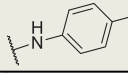
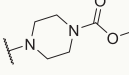
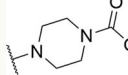
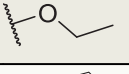
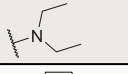
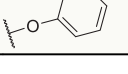
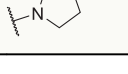
“Se” (**8a**) or “NH” (**8b**) nearly abolished the H₂S depletion activity. Interestingly, oxidation of the 5-N to N-oxide led to enhanced depletion potency (**9a**, **9b**, and **9d**), presumably due to the electron-withdrawing ability of the N-oxide group, making the C-4 position more liable for HS[−] addition. Again, the positive charge center at the leaving group was also indispensable for H₂S depletion for the N-oxide derivatives, as demonstrated by the weak depletion capacity of compounds **9c**, **9e**, and **9f**.

To further validate the H₂S scavengers obtained from the MB assay, compounds **7a–c**, **7g**, **7i**, **9a**, **9b**, and **9d** with decay half-lives below 10 min were screened for their H₂S-depletion potency in *S. aureus*, and all the tested compounds displayed an HPLC purity of over 95% (Supplementary Fig. 9). As shown in Fig. 3 and Supplementary Figs. 20, 21, most of the tested compounds showed H₂S-depletion activity in *S. aureus* with varying potency. Although **9b** and **9d** displayed very potent H₂S-depletion activity in the MB assay, they only exhibited minimum activity in *S. aureus*. Delightfully, compounds **7b** and **9a** displayed more potent activity than the hit compound **7a**. In addition, we also used MB assay to quantify the bacteria-derived H₂S and similar trends were observed (Supplementary Fig. 15). Compounds **7b** and **9a** exhibited very pronounced H₂S-depletion activity in such an assay as well. In addition, **7b** showed high selectivity for H₂S over glutathione, as no adduct was formed between **7b** and glutathione even after 24 h of incubation in 20% of acetonitrile/PBS (pH = 7.4) at 37 °C (Supplementary Fig. 11). Consequently, compounds **7b** and **9a** were selected for subsequent studies.

Antibacterial sensitization studies

Before moving to the antibacterial sensitization evaluation, compounds **7b** and **9a** were initially assayed to check whether they affect bacterial proliferation. H₂S is not essential for bacterial survival, and all bacteria survive after the knockout of H₂S-synthesizing enzymes³⁰. As expected, compound **7b** did not affect bacterial proliferation at concentrations up to 50 μ M (Supplementary Fig. 22). Interestingly, compound **9a** displayed some bactericidal effects against *S. aureus* (Supplementary Fig. 22), despite that it shared a very similar structure to **7b**. To determine if the bactericidal effects resulted from the byproduct between H₂S and **9a**, *S. aureus* was pretreated with H₂S-synthesizing enzyme inhibitors (PAG + AOAA) to deplete H₂S (Supplementary Fig. 22), and **9a** exhibited similar bactericidal effects

Table 1 | The H₂S decay half-lives in the presence of different derivatives

<div>  </div>									
Compound	R ₁	X	Y	t _{1/2} (min)	Compound	R ₁	X	Y	t _{1/2} (min)
7a		O	N	4	7j		O	N	12
7b		O	N	3	8a		Se	N	16
7c		O	N	3	8b		NH	N	19
7d		O	N	17	9a		O	N ⁺ -O ⁻	1
7e		O	N	18	9b		O	N ⁺ -O ⁻	1
7f		O	N	15	9c		O	N ⁺ -O ⁻	20
7g		O	N	9	9d		O	N ⁺ -O ⁻	1
7h		O	N	15	9e		O	N ⁺ -O ⁻	20
7i		O	N	7	9f		O	N ⁺ -O ⁻	20

in such cells, indicating that the bactericidal effects were mainly attributed to the scaffold of **9a** but not the H₂S-addition product. To better decipher the roles of H₂S in antibacterial sensitization and biofilm formation, compound **7b** was picked for subsequent in vitro and in vivo studies.

As shown in Fig. 4A, compound **7b** exhibited sensitizing effects in killing *S. aureus* with gentamicin (Gm), and the sensitizing effects were abolished by the addition of exogenous H₂S (Na₂S). In addition, the byproduct **22** from the reaction between H₂S and compound **7b** did not inhibit the proliferation of *S. aureus* and exhibited no similar sensitizing effects with Gm (Fig. 4B). The addition of CBS/CSE inhibitors PAG + AOAA did not further bolster the efficacy of Gm plus **7b** either (Fig. 4C). Noteworthy, the solution color of **7b** was yellow, which gradually turned into red upon mixing with *S. aureus*. This colorimetric change was primarily attributed to the reaction between **7b** and H₂S, which yielded compound **22** featuring a red color and an absorbance peak at 550 nm (Supplementary Figs. 12, 13)⁴⁶. This observation also provided another line of evidence to support that the downregulation of H₂S was mainly attributed to H₂S scavenging but not enzyme inhibition. In aggregate, it can be safely concluded that the observed sensitization effects were primarily attributed to the H₂S-depletion effects of compound **7b**. Next, we evaluated the bactericidal effects of **7b** in combination with other frequently used antibiotics. As expected, compound **7b** also sensitized *S. aureus* to the treatment of other bactericidal agents, including Cl (ciprofloxacin), Amp (ampicillin), Van (vancomycin) and Em (erythromycin), and all the sensitizing effects were reversed by the addition of exogenous H₂S (Fig. 4D–G). In addition, we also tested the cytotoxicity of compound **7b** toward

mammalian HEK293 cells. Appealingly, compound **7b** showed no obvious toxicity toward HEK293 cells at concentrations up to 200 μM. More importantly, compound **7b** did not increase the cytotoxicity of the antibiotics in HEK293 cells either (Supplementary Fig. 24).

Encouraged by the above-mentioned results, we move to examine if **7b** can efficiently deplete H₂S in other bacteria expressing varied H₂S-synthesizing enzymes. To this end, bacteria *P. aeruginosa* and drug-resistant bacteria *MRSA* were employed, both of which leverage CSE to produce H₂S. Meanwhile, *E. coli* carrying 3-MST as the main H₂S-synthesizing enzyme was also tested. As expected, compound **7b** efficiently scavenged H₂S in all these bacteria in a dose-dependent fashion (Supplementary Figs. 16, 17). In addition, compound **7b** also efficiently sensitized these bacteria to the treatment of Gm or Cl (Fig. 5A–D), and the sensitizing effects were reversed by the addition of exogenous H₂S, attributing the potentiation effects to the depletion of H₂S. To further validate that the potentiation effects of **7b** predominantly resulted from H₂S depletion, we carried out the same experiments in a *cbs/cse* knockout strain of *P. aeruginosa*. As shown in Supplementary Fig. 19., the *cbs/cse* knockout strain of *P. aeruginosa* did not produce detectable H₂S with the Pb(OAc)₂ paper strip assay, and as expected, **7b** can efficiently sensitize the wild-type strain of *P. aeruginosa* to the treatment of Gm and Cl (Fig. 5C, D and Supplementary Fig. 23), while failed to do the same in the *cbs/cse* knockout strain (Fig. 5E, F and Supplementary Fig. 23). These results unambiguously attributed **7b**'s potentiation effects to H₂S depletion.

The shared mechanism of action of different bactericidal agents was proposed to be reactive oxygen species (ROS)-inducing, and the protective roles of bacteria-derived H₂S were primarily due to its anti-

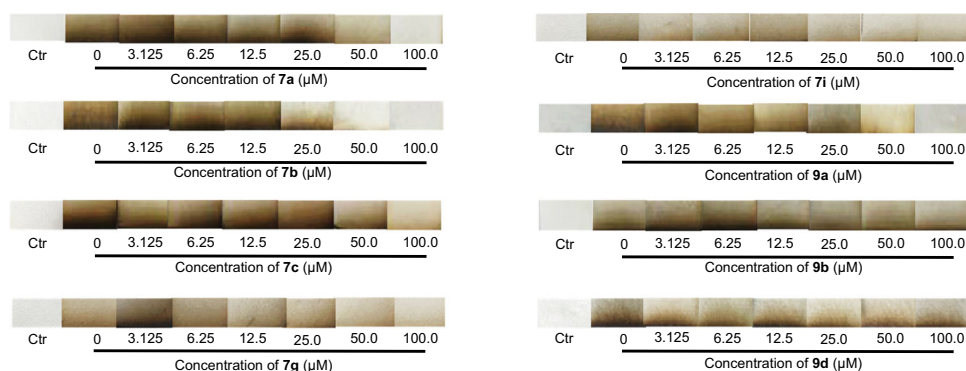


Fig. 3 | The H₂S-depletion activity of the selected H₂S scavengers in *S. aureus*. The H₂S concentration was semi-quantified by the lead acetate paper strip assay. Ctr refers to the control group without the bacteria.

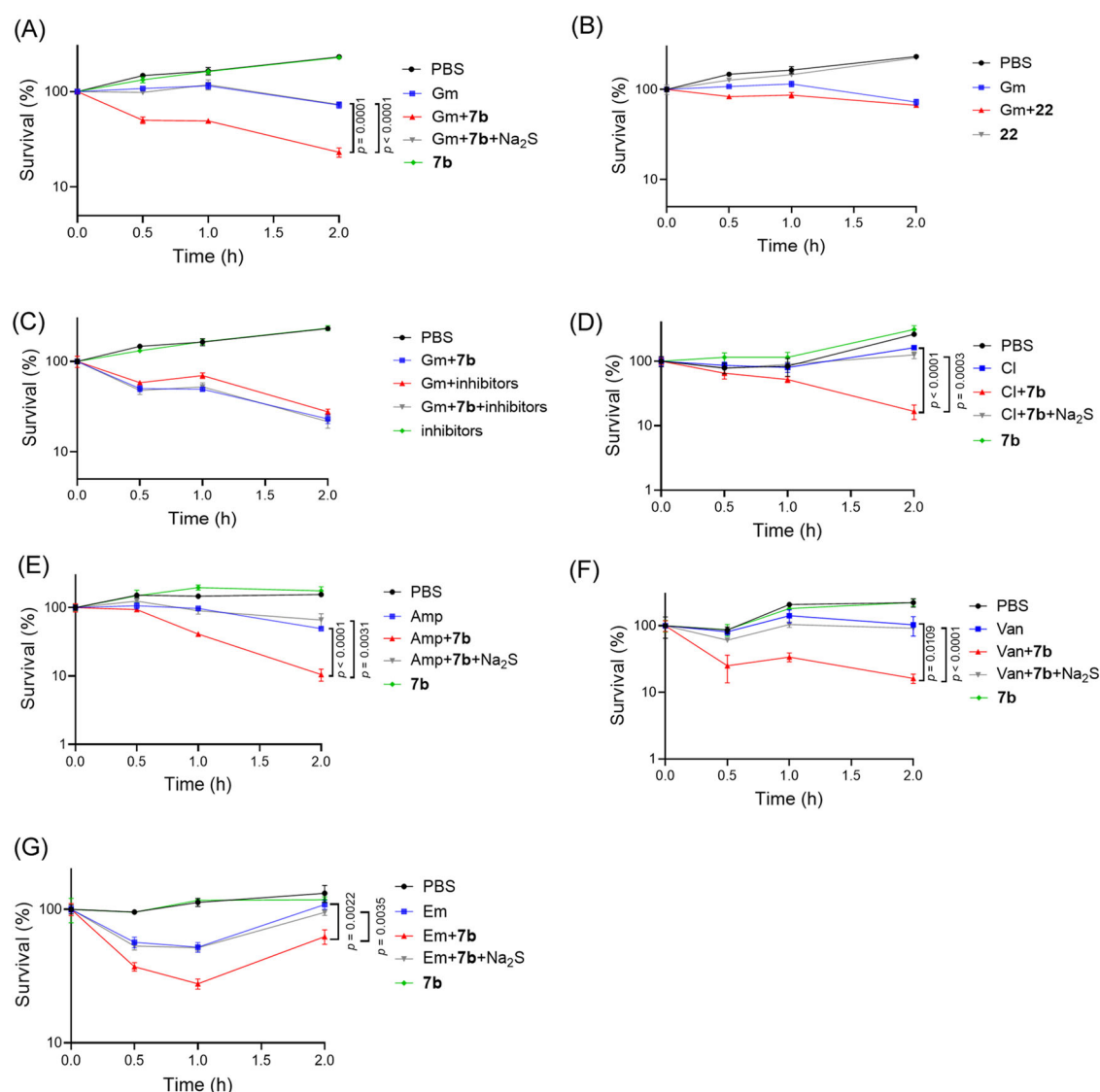


Fig. 4 | 7b sensitizes *S. aureus* to the treatment of antibiotics. **A** Sensitizing effects of compound 7b (25 μM) in killing *S. aureus* with Gm (0.23 μM). **B** Sensitizing effects of compound 22 (25 μM) in killing *S. aureus* with Gm (0.23 μM). **C** Sensitizing effects of compound 7b (25 μM) in killing *S. aureus* with Gm in the presence/absence of CBS/CSE inhibitors AOAA (50 μM) and PAG (0.5 mM). **D–G** Sensitizing

effects of compound 7b with ciprofloxacin (Cl, 0.88 μM, **D**), ampicillin (Amp, 5.80 μM, **E**), vancomycin (Van, 0.81 μM, **F**), and erythromycin (Em, 0.40 μM, **G**). The concentration of Na₂S added was 200 μM. The results are expressed as mean ± S.D. $n = 3$ biological replicates. One-way ANOVA followed by Tukey's post hoc analysis. Source data are provided as a Source Data file.

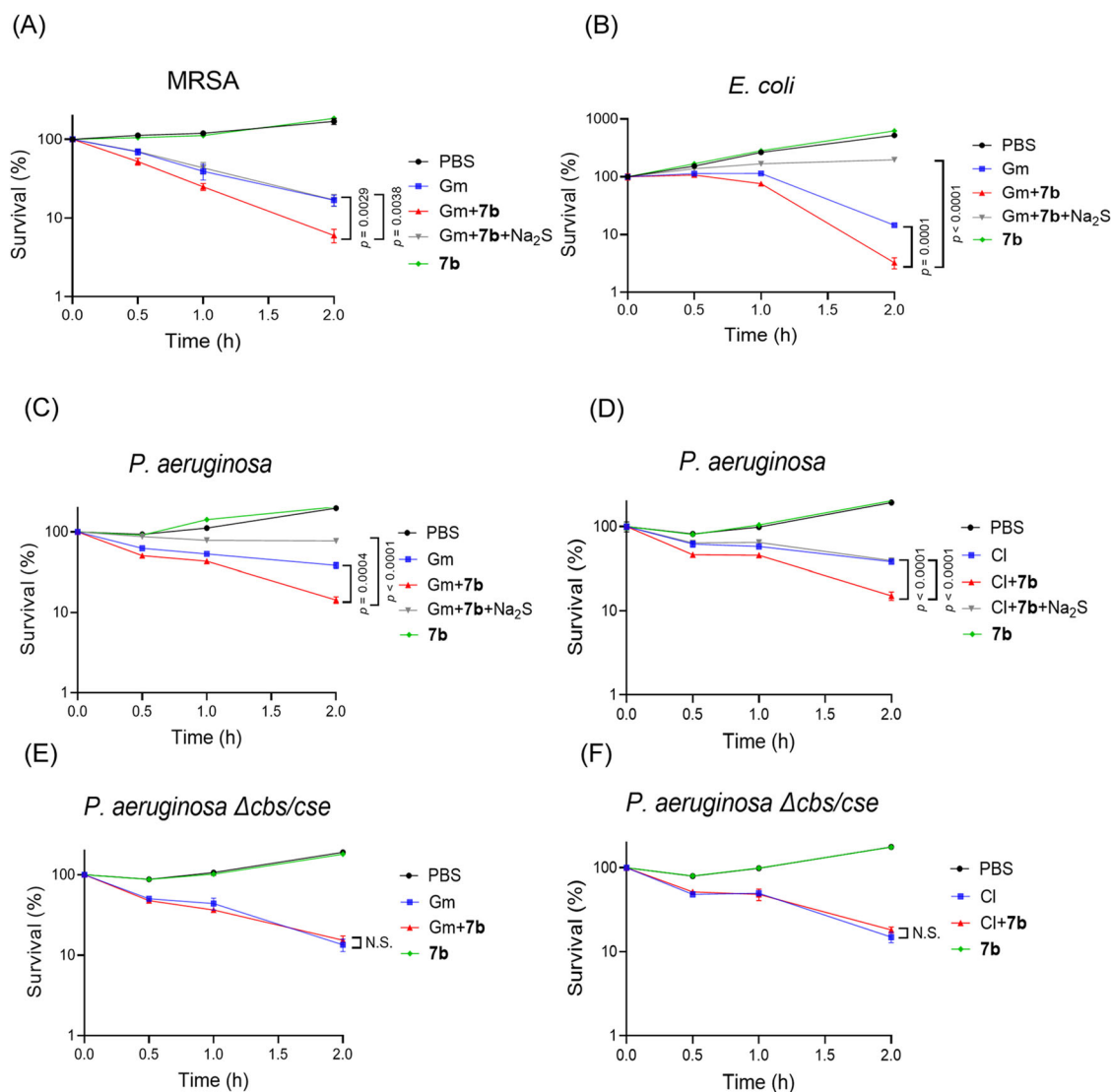


Fig. 5 | Compound 7b displays sensitizing effects with antibiotics in killing different strains of bacteria. The concentration of compound 7b is 25 μ M. **A** MRSA (2.5 μ M Gm), **B** *E. coli* (0.98 μ M Gm), **C**, **D** wild-type *P. aeruginosa* (0.61 μ M Gm; 0.15 μ M Cl), **E**, **F** *cbs/cse* knockout *P. aeruginosa* (0.61 μ M Gm; 0.15 μ M Cl). The

concentration of Na₂S added was 200 μ M. The results are expressed as mean \pm S.D. $n = 3$ biological replicates. N.S.: not significant, compared to the control group. One-way ANOVA followed by Tukey's post hoc analysis. Source data are provided as a Source Data file.

oxidant effects by the inhibition of the Fenton reaction and/or activation of some antioxidant enzymes^{47,48}. Therefore, we speculate that compound 7b should be efficient in potentiating photodynamic therapy against H₂S-producing bacteria, which kills bacterial cells mainly by the light-induced generation of cytotoxic ROS. As shown in Fig. 6, a clinically approved photosensitizer chlorin e6 (**Ce6**) plus photo-irradiation exhibited bactericidal effects against *S. aureus*, *P. aeruginosa*, *E. coli*, and MRSA to different extents, and the cotreatment of 7b boosted the efficacy of **Ce6**, while no such effects were observed in the dark, suggesting the benefits of H₂S-depletion in photodynamic therapy.

H₂S is widely known as a potent anti-inflammatory agent in mammals by inhibiting the production of pro-inflammatory cytokines⁴⁹, which may hamper the bacterial clearance of the host. Indeed, evidence has shown that bacteria-derived H₂S suppressed the immune response of the host, and the inhibition of H₂S-biogenesis enhanced the clearance of bacteria by macrophages⁵⁰. Therefore, we also tested the effects of compound 7b on the capacity of macrophages to clear bacteria. As shown in Fig. 7, compound 7b indeed enhanced the clearance of *S. aureus*, *E. coli*, and *P. aeruginosa* in

macrophage cells. In addition, 7b failed to bolster macrophage-mediated clearance of the *cbs/cse* knockout *P. aeruginosa* strain at the time point of 1 h and 2 h, albeit some sensitizing effects were observed at 0.5 h, indicating that the enhanced bacteria clearance was mainly ascribed to H₂S depletion. Expectedly, the treatment of 7b slightly elevated the TNF- α level in *P. aeruginosa*-challenged macrophages (Supplementary Fig. 25). Moreover, 7b was also able to enhance the clearance of the wild-type but not the *cbs/cse* knockout *P. aeruginosa* in polymorphonuclear neutrophils (PMNs, Fig. 7D).

Persisters are a class of metabolically less active bacterial cells that primarily reside within the biofilm and, thus, are relatively hard to kill. Previous observations indicated that persisters possess relatively high levels of H₂S, which inhibits the synthesis of ATP by inactivating heme-copper terminal oxidases. However, H₂S spares the activity of cytochrome bd oxidases, sustaining the growth and respiration of bacteria albeit at a low ATP level⁵¹, thus leading to slow metabolism and high tolerance. In addition, H₂S is also demonstrated to contribute to the formation of biofilm, and the inhibition of CSE disrupts the formation of biofilm and thus sensitizes the persisters to the bactericidal agents³¹. Therefore, we move to test if compound 7b would elicit the same

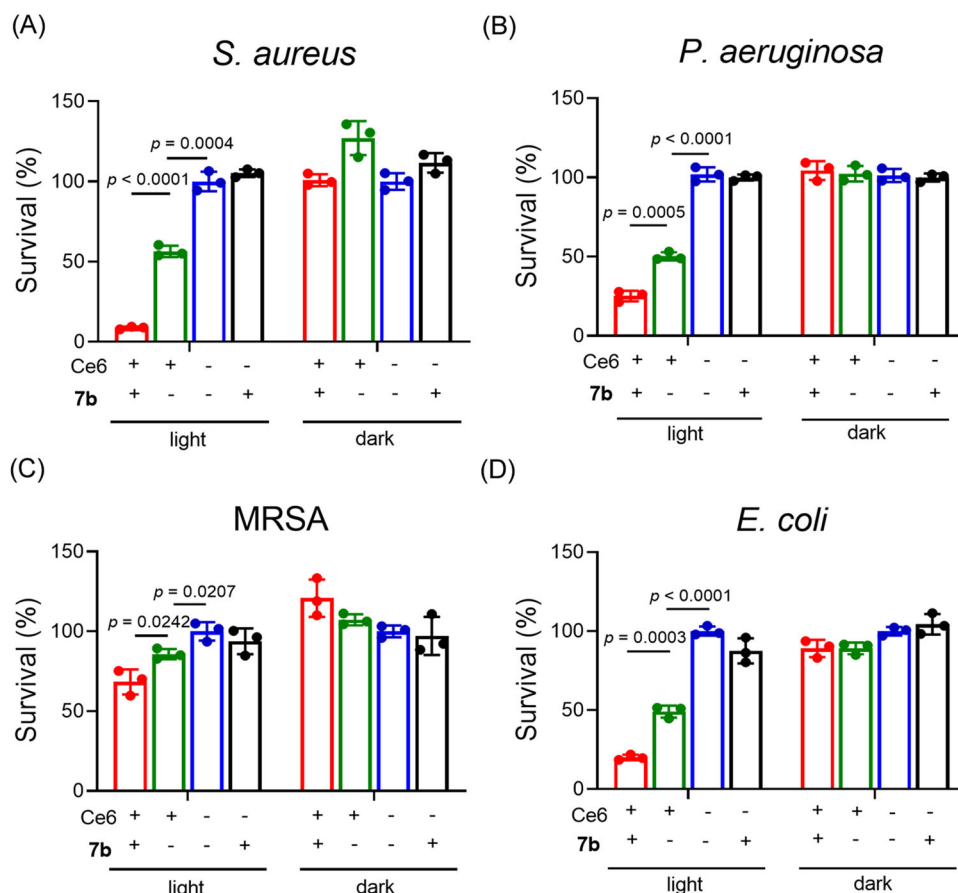


Fig. 6 | Compound 7b displays sensitizing effects with photosensitizer Ce6 in killing different strains of bacteria. **A** Ce6 (1.68 μM), 7b (25 μM). Photoirradiation was performed with a 665 nm laser (0.1 mW cm^{-2} for 40 s, energy density is 4 J cm^{-2}). **B** Ce6 (33.5 μM), 7b (25 μM). Photoirradiation was performed with a 665 nm laser (1 mW cm^{-2} for 180 s, energy density is 180 J cm^{-2}). **C** Ce6 (16.8 μM), 7b (25 μM). Photoirradiation was performed with a 665 nm laser (1 mW cm^{-2} for 60 s,

energy density is 60 J cm^{-2}). **D** Ce6 (16.8 μM), 7b (25 μM). Photoirradiation was performed with a 665 nm laser (1 mW cm^{-2} for 90 s, energy density is 90 J cm^{-2}). The results are expressed as mean \pm S.D. $n = 3$ biological replicates. One-way ANOVA followed by Tukey's post hoc analysis. Source data are provided as a Source Data file.

phenotypes. As shown in Fig. 8, compound 7b not only efficiently inhibited the formation of biofilm, but also eradicated the formed biofilm in both strains of *S. aureus* and *P. aeruginosa*, and such effects were reversed by the addition of exogenous H_2S . In addition, the depletion of the *cbs/cse* gene in *P. aeruginosa* significantly compromised the biofilm formation, and the treatment of 7b did not further enhance the biofilm inhibition and eradication (Fig. 8A, B). Although 7b did not affect the proliferation of bacteria, it displayed the capacity to eradicate formed biofilm. One possible explanation for this observation is that the depletion of H_2S inhibits the production of biofilm component(s) without altering bacterial viability. For example, H_2S was reported to keep pyocyanin in the reduced form in *P. aeruginosa*³¹. Pyocyanin is associated with biofilm formation and stabilization^{52,53}, and the downregulation of H_2S via CSE inhibition was able to decrease the pyocyanin level, leading to biofilm disruption³¹. Next, we set out to probe if 7b could also sensitize persister cells to the treatment of antibiotics by employing a well-accepted anti-persister assay⁵⁴. Expectedly, Gm and Cl displayed minimum bactericidal effects against the persisters underneath the biofilm (Fig. 8C). However, the addition of compound 7b sensitized both strains of persisters toward the treatment of Gm and Cl, indicating the benefits of biofilm disruption in eradicating persisters. Again, the knockout of the *cbs/cse* gene in *P. aeruginosa* significantly sensitized the persister cells to Gm, and 7b did not further potentiate Gm in such a mutant strain. Taking together, these results indicated that 7b inhibited the biofilm formation and sensitized persisters predominantly via H_2S depletion.

In vivo antibacterial sensitization

Having confirmed the H_2S depletion and antibacterial sensitization capacity of compound 7b in vitro, we move to examine if compound 7b can recapitulate the same effects in vivo. Toward this end, an acute *P. aeruginosa*-infected pneumonia mouse model was employed. The mice were inoculated with either wild-type or mutant *P. aeruginosa* via intranasal route at 5×10^5 colony-forming units (CFU). After 0.5 h, the mice were treated subcutaneously with 7b (20 mg/kg) plus Gm (20 mg/kg), Gm (20 mg/kg), 7b (20 mg/kg), or the vehicle. After 24 h, the mice were sacrificed, and the lung homogenate and bronchoalveolar lavage fluid (BALF) were collected to quantify the bacterial colonies. As shown in Fig. 9, in the mice infected with the wild-type *P. aeruginosa*, Gm alone displayed some antibacterial effects in the lung. Appealingly, the cotreatment of 7b and Gm significantly ameliorated the bacterial burden both in the lung homogenate and BALF, indicating a sensitizing effect between Gm and 7b. On the other hand, in the mice infected with the *cbs/cse* knockout *P. aeruginosa*, no sensitizing effects were observed between Gm and 7b. Altogether, these results demonstrated that the sensitizing effects predominantly resulted from the H_2S -depletion capacity of 7b. Noteworthy, the mice infected with the mutant bacteria displayed much lower bacterial colonies (ca. 1 log lower) in the lung as compared to their counterparts infected with the wild-type one. This observation is not surprising in that the *cbs/cse* knockout strain is more liable to macrophage-mediated clearance than the wild-type strain⁵⁰. However, 7b alone did not result in any reduction in bacterial colonies in the lung as compared to the vehicle group, even

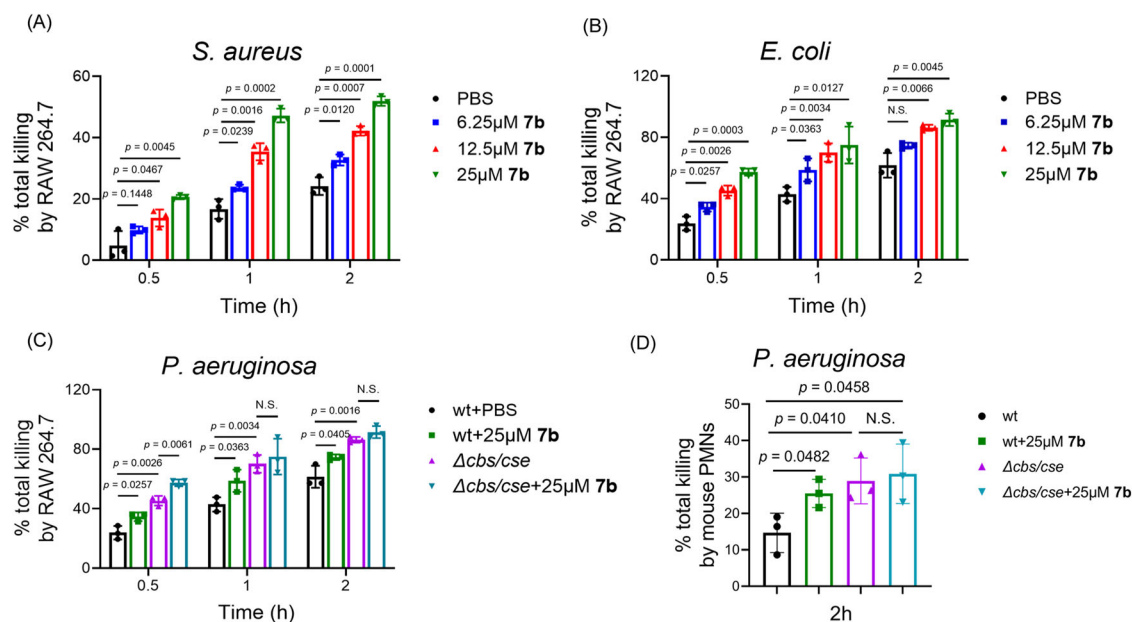


Fig. 7 | 7b boosts the intracellular bacterial clearance of macrophages and polymorphonuclear neutrophils. The effects of **7b** on the intracellular bacterial clearance in RAW264.7 cells (A–C) and PMNs (D), *S. aureus*, *E. coli*, or *P. aeruginosa* was cultured in the presence of **7b** before the inoculation of mouse leukocytes or PMNs. The graph shows bacterial elimination after 0.5 h, 1 h, or 2 h of coculture. The results are expressed as mean \pm S.D. $n = 3$ biological replicates. N.S.: not significant, compared to the control group. One-way ANOVA followed by Tukey's post hoc

analysis. For macrophages, the total killing was calculated according to the formula: $(N_0 - N)/N_0 \times 100\%$, wherein N_0 and N refer to the number of colonies at 0 h and different time points, respectively; For PMNs, the total killing was calculated according to the formula: $(N^0 - N)/N^0 \times 100\%$, wherein N^0 refers to the colony counts without neutrophils, while N denotes the colony counts within the treatment group. Source data are provided as a Source Data file.

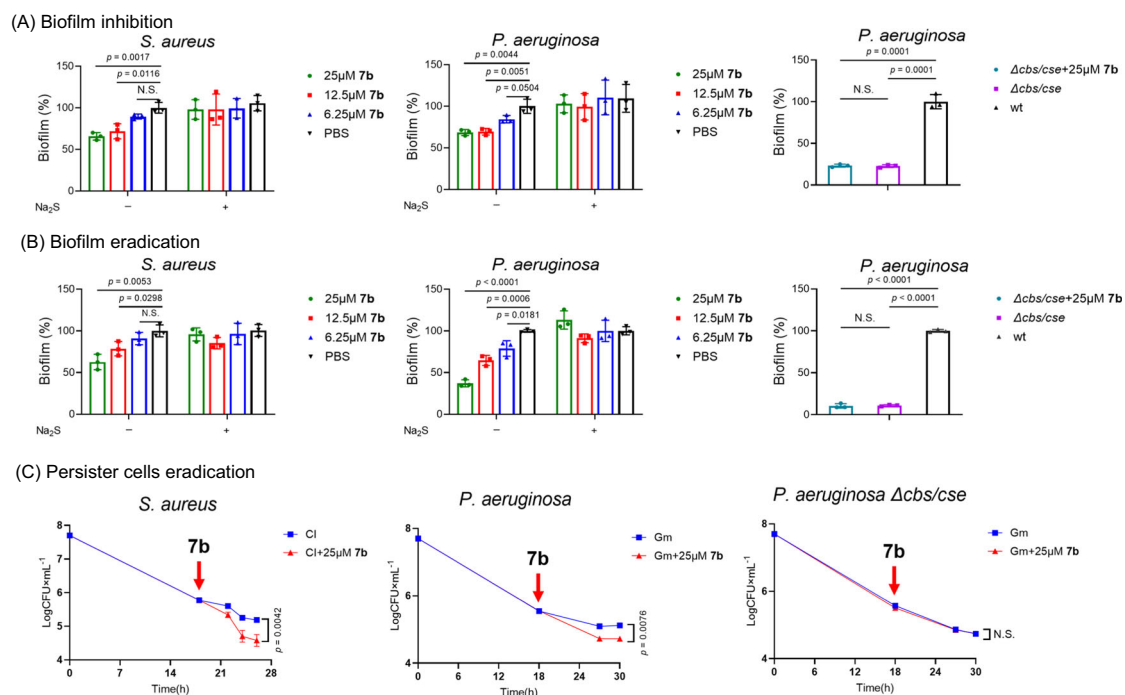


Fig. 8 | 7b disrupts the biofilm formation and sensitizes persisters to anti-biotics. **A** The biofilm inhibition by compound **7b** in *S. aureus* and *P. aeruginosa*. **B** The effects of H₂S scavengers **7b** on the removal of biofilm in *S. aureus* and *P. aeruginosa*. **C** The sensitization effects of **7b** on persister cells. CI (8.8 μM for *S. aureus*), Gm (24.5 μM for *P. aeruginosa*), N.S., not significant, compared to the

bacteria group. The results are expressed as mean \pm S.D. $n = 3$ biological replicates. One-way ANOVA followed by Tukey's post hoc analysis. The PBS treatment group was set to 100%, and the other groups were normalized *vs* the control group. Source data are provided as a Source Data file.

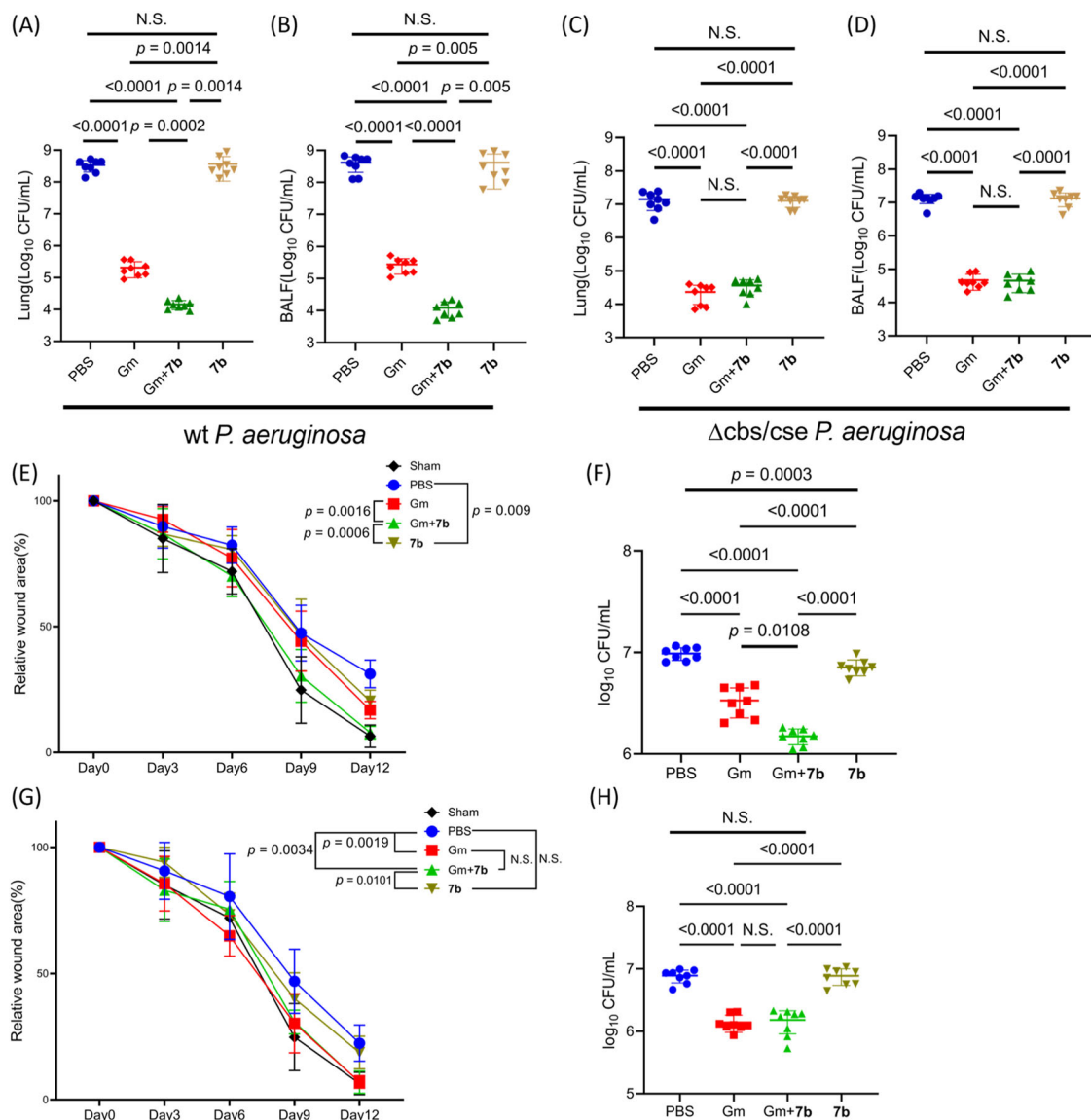


Fig. 9 | 7b displays sensitizing effects with Gm in vivo. A–D Therapeutic effects of H₂S scavenger 7b in combination with Gm in a *P. aeruginosa*-infected pneumonia mouse model. Bacterial burden in the lung homogenate (A, C) and BALF (B, D) from different treatment groups. The results are expressed as mean \pm S.D. $n = 8$ biological replicates. N.S.: not significant, compared to the control group.

E–H Therapeutic effects of H₂S scavenger 7b in combination with Gm in a *P. aeruginosa*-infected skin wound mouse model. Relative wound area and bacterial

burden from different treatment groups in the wt *P. aeruginosa* (E, F) and mutant *P. aeruginosa* (G, H) infected mice. The sham groups in (E) and (G) are the same. N.S.: not significant, compared to the control group on day 12. The results are expressed as mean \pm S.D. $n = 5$ biological replicates for Fig. 9E and G, $n = 8$ biological replicates for Fig. 9F and H. One-way ANOVA followed by Tukey's post hoc analysis. Source data are provided as a Source Data file.

though it was expected to deplete H₂S. One possible explanation is that the dosage of 7b (20 mg/kg) employed is not enough to lower the H₂S level to such an extent for immune system-mediated antibacterial sensitization. The other possibility is that H₂S exhibits a biphasic effect on the immune system⁵⁵. Studies indicated that low concentrations of endogenous H₂S promoted the chemotaxis of macrophages⁵⁶. Since 7b has no targetability, it is likely to deplete endogenous H₂S in the immune system as well and thus affects the migration of macrophages. Therefore, the enhancement of macrophage-mediated bacterial clearance in the lung is probably offset by the penalty of possibly decreased numbers of macrophages in the lung.

To further validate 7b's effects in vivo, we tested its efficacy in a *P. aeruginosa*-infected skin wound mouse model. As expected, the group receiving 7b (20 mg/kg) and Gm (1 mg/kg) displayed lower bacteria colonies and smaller wound areas than the group receiving Gm (1 mg/kg) only in mice infected with wt *P. aeruginosa* (Fig. 9E, F), indicating a

sensitizing effect between Gm and 7b, while no such effects were observed in mice infected with the mutant *P. aeruginosa* (Fig. 9G, H). Unlike the systemic administration of 7b in the pneumonia mouse model, 7b was locally administered in this model, and thus it could specifically deplete H₂S in the infection area without disturbing the endogenous H₂S level in other organs. Therefore, the locally administered 7b was expected to enhance the macrophage-mediated bacterial clearance without affecting the normal response of the immune system. Indeed, the 7b monotherapy group also exhibited relatively lower bacteria colonies and smaller wound areas than the vehicle group in mice infected with wt *P. aeruginosa*, while 7b failed to do the same in mice infected with the mutant *P. aeruginosa* (Fig. 9E–H). These results indicated that the antibacterial efficacy of 7b in vivo was mostly attributed to its H₂S-depletion activity. This observation also provides another line of evidence to support our speculation that the lack of efficacy of 7b in the pneumonia mouse model is likely due to unspecific depletion of

endogenous H₂S in other organs. It is worth mentioning that no anti-bacterial effects were observed with systemic administration of the CSE inhibitor in Nudler's work either³¹. However, the effects of H₂S on the immune system are very complicated, and mixed results are reported in this field⁵⁵. Whether this aspect accounts for **7b**'s divergent behaviors in these two animal models warrants further in-depth studies.

Discussion

Targeting bacterial tolerance is an effective strategy to reduce treatment failures in acute infections and lower the possibility of recurrence and transition to chronicity. Bacterial H₂S biogenesis is emerging as an important "tolerance pathway" for antibacterial adjuvant development, and the inhibitors of H₂S biogenesis have been demonstrated to sensitize bacteria and persists to bactericidal agents. However, due to the existence of three enzymes, inhibitors against one specific isoenzyme can not be applied in all situations. The development of pan-inhibitors against all the enzymes is highly demanded but represents an exceedingly challenging task. Moreover, there might also exist non-enzymatic pathways for H₂S production in bacteria.

To develop a broad-spectrum strategy to eliminate H₂S irrespective of the source of H₂S, we decided to deplete the end product H₂S chemically by devising specific scavengers, which were expected to eliminate H₂S in all H₂S-producing bacteria and would not raise the concern of resistance because they did not act on the enzymes. After the screening of chemically diversified scaffolds and a medicinal chemistry effort, compound **7b** was successfully identified as a versatile H₂S-scavenging reagent in H₂S-producing bacteria. Such an H₂S scavenger efficiently sensitized H₂S-producing bacteria, including *S. aureus*, *P. aeruginosa*, *E. coli*, and MRSA to bactericidal reagents as well as photodynamic therapy, boosted the bacterial clearance of macrophages, disrupted the formation of biofilm and sensitized the persisters to antibiotics. Importantly, such an H₂S scavenger displayed sensitizing effects with Gm in *P. aeruginosa*-infected pneumonia and skin wound mouse models. In addition, **7b** did not exhibit any sensitizing effects with antibiotics in killing the *cbh/cse* knockout strain of *P. aeruginosa* both in vitro and in vivo, confirming that **7b**'s sensitizing effects predominantly resulted from H₂S depletion. These results firmly established H₂S scavengers as an alternative strategy to deplete bacteria-derived H₂S for antibacterial sensitization and tolerance targeting, and compound **7b** represented a promising starting point for further antibacterial adjuvant development.

It is worth pointing out that ROS production may not be the primary killing mechanism of antibiotics, and this is likely the underlying reason for the observation that only around 1-log antibacterial killing of potentiation is achieved with H₂S depletion⁵⁷. Therefore, more profound sensitization effects might be obtained by combining **7b** with other antibacterial therapies, which kill bacteria mainly via ROS production (i.e., photodynamic therapy). In addition, because endogenous H₂S plays indispensable physiological roles in mammals, the indiscriminate depletion of mammalian cell-derived H₂S may raise safety concerns. However, it may be argued that the depletion of H₂S in mammalian cells may stimulate the compensation pathway to maintain normal functions. For example, the triumvirate of gasotransmitters (CO, H₂S, and NO) share similar effects in several aspects, act on the same transduction pathways, and show crosstalk among each other⁵⁸. Therefore, the transient depletion of H₂S might not lead to severe side effects. Nevertheless, the toxicity profiles of **7b** and its analogs must be investigated systemically in the future.

As for the mechanism(s) underlying **7b**-enhanced bacterial clearance of macrophages/PMNs, the reported results indicated that the enhanced phagocytosis was likely attributed to immune responses, but the specific immunological mechanisms involved remain to be elucidated⁵⁰. In addition, it is also plausible that the enhanced bacterial clearance is associated with the impaired

bacterial detoxification of ROS generated by macrophages. Moreover, the effects of H₂S on the immune system are very complicated, and mixed results are reported in this field. As such, it is challenging to deconvolute the interactions between H₂S and the immune system. However, it is now generally accepted that the effects of H₂S on the immune system are concentration-specific, and it can either activate or suppress the host immune response at different concentrations. Considering the complexity of the host immune system and its interactions with H₂S, intensive efforts are demanded to delineate **7b**'s effects on the immune system in future studies. Meanwhile, what is left for future work also includes how H₂S attenuates antibiotic killing beyond the direct reaction of a thiol persulfide with the beta-lactams⁵⁹ and its antioxidant effects. For example, it would be interesting to dig into whether H₂S can activate the activity of certain biofilm regulators (i.e., BfmR and Crp) via persulfidation to facilitate biofilm formation⁶⁰.

Noteworthy, some mixed results were reported regarding the effects of H₂S on the growth of bacteria. For example, it was reported that exogenous H₂S stimulated the production of ROS and decreased glutathione (GSH) levels in *E. coli*, resulting in lipid peroxidation and DNA damage⁶¹, inhibited the biofilm formation of *Streptococcus mitis* and *Streptococcus oralis*⁶², and sensitized *Acinetobacter baumannii* to antibiotics⁶³. The underlying reasons for such divergent behaviors of H₂S are speculated to be at least two-fold: (1) the effects of H₂S on bacteria might be strain-specific. H₂S is cytotoxic in some strains, especially those without endogenous H₂S generation (i.e., *Acinetobacter baumannii*⁶⁰), while it is cytoprotective in others. (2) H₂S is featured with biphasic pharmacological effects, which means opposite phenotypes are noticed at different concentrations. It is worth pointing out that the antibacterial phenotype of H₂S was mostly observed at relatively high concentrations (0.25–5 mM). It is thus reasonably speculated that at low physiological concentrations, H₂S mainly functions as a cytoprotective reagent against antibiotic insult, while becoming cytotoxic at elevated concentrations. Nevertheless, at least in the strain of *S. aureus*, *P. aeruginosa*, *E. coli*, and MRSA, our results provided another layer of evidence to support the multifunctional protective roles of bacteria-derived H₂S and established H₂S biogenesis as a very promising target for antibacterial adjuvant design to combat tolerance and resistance.

Methods

Chemistry

General. All reagents and solvents were of reagent grade. Column chromatography was carried out on silica gel (Sorbent 200–300 mesh), or neutral alumina (Sorbent 200–300 mesh). TLC analysis was conducted on silica gel plates (Sorbent Silica G UV254). NMR spectra were recorded on 300 or 400 MHz spectrometers (Brker, AVANCE NEO 400 MHz; Ajilent, vnmrs-300MHz). Chemical shifts (δ values) and coupling constants (J values) are given in ppm and hertz, respectively, using the respective solvent (¹H NMR, ¹³C NMR) as the internal reference. HPLC analysis was performed on Ultra-fast, High-performance Liquid Chromatography (UFLC, Shimadzu, SPD-20A).

General procedure A

To a solution of 4-chloro-7-nitrobenzofurazan (NBD-Cl, 1.1 equiv) in CH₂Cl₂ (5 mL) was added the nucleophile (1.0 equiv.) and base (Et₃N, DIPEA or CH₃ONa, 1.5–3.0 equiv.). The obtained reaction mixture was stirred for 1–12 h at room temperature. Then the reaction mixture was poured into 20 mL water and was extracted with CH₂Cl₂ (3 × 20 mL). The obtained organic layer was then dried over Na₂SO₄. After filtration and concentration, the obtained crude product was purified by chromatography on silica gel or neutral alumina with methanol/dichloromethane to give the products.

The synthesis of compound 7a

Compound **7a** was synthesized following the general procedure A (100 mg, 83%). ¹H NMR (400 MHz, CDCl₃) δ 8.44 (d, *J* = 8.9 Hz, 1H), 6.32 (d, *J* = 8.9 Hz, 1H), 4.13 (s, 4H), 2.68 (s, 4H), 2.40 (s, 3H).

The synthesis of compound 10

To a solution of 1-methylpiperazine (500 mg, 4.99 mmol) in THF (6 mL) was added di-*tert*-butyl dicarbonate (1.38 mL, 5.99 mmol) under 0 °C, and the resulting mixture was stirred at room temperature for 2 h. Then the reaction fluid was poured into 20 mL water. The mixture was extracted with CH₂Cl₂, and the obtained organic layer was then dried over Na₂SO₄. After filtration and concentration, the obtained crude product was purified by chromatography on silica gel with methanol/dichloromethane (1/30, v/v) to give a brown-black solid product **10** (920 mg, 92%). ¹H NMR (400 MHz, CDCl₃) δ 3.43 (s, 4H), 2.34 (s, 4H), 2.29 (d, *J* = 1.1 Hz, 3H), 1.45 (d, *J* = 1.0 Hz, 9H).

The synthesis of compound 11

Methyl triflate (163.87 mg, 0.99 mmol) was added dropwise to a solution of **10** (100 mg, 0.50 mmol) in dry CH₂Cl₂ (5 mL) under 0 °C, and the resulting mixture was stirred at room temperature for 1 h. After that, the mixture was treated with triflic acid (113.86 mg, 0.99 mmol) under 0 °C and was stirred at room temperature for another 1 h. The solvent was removed under reduced pressure, and the resulting residue was triturated with 5 mL methanol to produce a white solid precipitate **11** (113 mg, 86%). ¹H NMR (400 MHz, D₂O) δ 3.79 (d, *J* = 4.9 Hz, 4H), 3.73 (s, 4H), 3.34 (s, 6H).

The synthesis of compound 7b

Compound **7b** was synthesized following the general procedure A using NBD-Cl and **11** as the starting material. brown-black solid product. (35 mg, 47%). ¹H NMR (400 MHz, D₂O) δ 8.50 (d, *J* = 8.8 Hz, 1H), 6.62 (d, *J* = 8.8 Hz, 1H), 4.47 (s, 4H), 3.79 (s, 4H), 3.35 (s, 6H).

The synthesis of compound 7d

Compound **7d** was synthesized according to the general procedure A as a red solid product (59 mg, 87%). ¹H NMR (400 MHz, CDCl₃) δ 8.44 (d, *J* = 8.6 Hz, 1H), 7.73 (s, 1H), 7.30 (d, *J* = 5.9 Hz, 4H), 6.64 (d, *J* = 8.6 Hz, 1H), 2.42 (s, 3H).

The synthesis of compound 7e

Compound **7e** was synthesized according to the general procedure A as a red solid product (40 mg, 67%). ¹H NMR (400 MHz, CDCl₃) δ 8.44 (d, *J* = 9.1 Hz, 1H), 6.13 (d, *J* = 9.1 Hz, 1H), 3.96 (s, 4H), 1.40 (t, *J* = 7.1 Hz, 6H).

The synthesis of compound 7f

Compound **7f** was synthesized according to the general procedure A as a red solid (45 mg, 68%). ¹H NMR (400 MHz, CDCl₃) δ 8.44 (d, *J* = 8.9 Hz, 1H), 6.01 (d, *J* = 9.0 Hz, 1H), 4.31 (s, 2H), 3.65 (s, 2H), 2.48 – 2.04 (m, 4H).

The synthesis of compound 7h

Compound **7h** was synthesized according to the general procedure A as a yellow solid product (40 mg, 38%). ¹H NMR (400 MHz, CDCl₃) δ 8.13 (d, *J* = 9.8 Hz, 1H), 7.50 (d, *J* = 9.8 Hz, 1H), 4.48 (q, *J* = 7.0 Hz, 2H), 1.56 (s, 3H).

The synthesis of compound 7i

Compound **7i** was synthesized according to the general procedure A as a yellow solid product (40 mg, 15%). ¹H NMR (400 MHz, CDCl₃) δ 8.43 (d, *J* = 8.3 Hz, 1H), 7.54 (d, *J* = 8.1 Hz, 2H), 7.42 (t, *J* = 7.4 Hz, 1H), 7.27 (t, *J* = 3.9 Hz, 2H), 6.53 (d, *J* = 8.3 Hz, 1H).

The synthesis of compound 7j

Compound **7j** was synthesized according to the general procedure A as an orange solid product (50 mg, 37%). ¹H NMR (400 MHz, CDCl₃) δ

8.43 (d, *J* = 9.0 Hz, 1H), 6.12 (d, *J* = 9.0 Hz, 1H), 4.22 (s, 2H), 3.50 (s, 3H), 2.67 (t, *J* = 6.9 Hz, 2H), 2.32 (s, 6H).

The synthesis of compound 12

Compound **12** was synthesized following the general procedure A as an orange solid product. ¹H NMR (400 MHz, CDCl₃) δ 8.47 (s, 1H), 6.31 (s, 1H), 4.12 (s, 4H), 3.74 (s, 4H), 1.52 (s, 9H).

The synthesis of compound 13

The solution containing **12** (200 mg, 0.57 mmol) in CH₂Cl₂ (5 mL) was treated with trifluoroacetic acid (0.22 mL, 2.86 mmol) under 0 °C, and the resulting mixture was stirred at room temperature for 1 h. The solvent was removed under reduced pressure, and the obtained residue was triturated with 5 mL diethyl ether to produce a white solid precipitate **13** (200 mg, 96%). ¹H NMR (400 MHz, DMSO-*d*₆) δ 9.30 (s, 2H), 8.61 (d, *J* = 8.9 Hz, 1H), 6.80 (d, *J* = 9.0 Hz, 1H), 4.34 (s, 4H), 3.44 (s, 3H).

The synthesis of compound 7c

To a solution of **13** (49.36 mg, 0.14 mmol) in CH₂Cl₂ (1 mL) was added 2-chloro-1-methylpyridinium iodide (34.71 mg, 0.14 mmol) and triethylamine (41.25 mg, 0.41 mmol). The reaction mixture was stirred for 12 hours at room temperature. After completion of the reaction, the reaction solution was filtered, and the filtrate was concentrated under reduced pressure. The obtained residue was purified by chromatography on neutral alumina with methanol/dichloromethane (1/10, v/v) to give a dark-red solid product **7c** (25 mg, 54%). ¹H NMR (400 MHz, DMSO-*d*₆) δ 8.64 (dd, *J* = 6.4, 1.5 Hz, 1H), 8.56 (d, *J* = 9.1 Hz, 1H), 8.40 – 8.28 (m, 1H), 7.69 (d, *J* = 8.2 Hz, 1H), 7.61 – 7.47 (m, 1H), 6.74 (d, *J* = 9.2 Hz, 1H), 4.37 (s, 4H), 4.15 (s, 3H), 3.80 – 3.60 (m, 4H).

The synthesis of compound 7g

To a solution of **13** (100 mg, 0.28 mmol) in CH₂Cl₂ (5 mL) was added propyl chloroformate (50.60 mg, 0.41 mmol) and triethylamine (55.71 mg, 0.55 mmol). The reaction mixture was stirred for 1 h at room temperature. After completion of the reaction, the reaction solution was concentrated under reduced pressure, and the obtained residue was purified by chromatography on silica gel with dichloromethane to give a dark-red solid product **7g** (40 mg, 43%). ¹H NMR (400 MHz, CDCl₃) δ 8.45 (d, *J* = 8.8 Hz, 1H), 6.32 (d, *J* = 8.9 Hz, 1H), 4.12 (t, *J* = 6.7 Hz, 6H), 3.92 – 3.68 (m, 4H), 1.70 (dd, *J* = 14.2, 6.9 Hz, 2H), 0.98 (t, *J* = 7.4 Hz, 3H).

The synthesis of compound 14

To a solution of 2, 3-diaminofluorobenzene (1 g, 7.93 mmol) in EtOH (20 mL) was added selenium dioxide (1.06 g, 9.51 mmol). The reaction mixture was heated under reflux for 1 h. After completion of the reaction, the solvent was removed under reduced pressure, and the residue was purified by chromatography on silica gel with ethyl acetate/petroleum ether (1/5, v/v) to give a white solid product **14** (1.36 g, 85%). ¹H NMR (300 MHz, CDCl₃) δ 7.66 (d, *J* = 9.1 Hz, 1H), 7.44 (dd, *J* = 13.5, 8.0 Hz, 1H), 7.14 – 6.91 (m, 1H).

The synthesis of compound 15

To a solution of **14** (460 mg, 2.29 mmol) in H₂SO₄ (5 mL) was added HNO₃ (1.5 mL) dropwise at 0 °C. After the completion of the addition, the reaction mixture was warmed to room temperature and stirred for another 1 h. After that, the reaction was quenched with H₂O (50 mL), and a yellow precipitate was formed. The mixture was extracted with EtOAc (3 × 50 mL), and the combined organic layer was dried over Na₂SO₄. After filtration and concentration, the obtained crude product was purified by chromatography on silica gel with ethyl acetate/petroleum ether (1/5, v/v) to give a yellow solid product **15** (430 mg, 76%). ¹H NMR (300 MHz, CDCl₃) δ 8.83 – 8.36 (m, 1H), 7.29 (d, *J* = 8.5 Hz, 1H).

The synthesis of compound 8a

To a solution of **15** (35 mg, 0.14 mmol) in acetonitrile (2 mL) was added compound **11** (37.59 mg, 0.14 mmol). The reaction mixture was stirred for 10 h at room temperature. After completion of the reaction, the solvent was removed under reduced pressure, and the crude product was purified by chromatography on neutral alumina with methanol/dichloromethane (1/10, v/v) to give a dark red solid product **8a** (43 mg, 61%). ¹H NMR (300 MHz, DMSO-*d*₆) δ 8.62 (d, *J* = 8.8 Hz, 1H), 6.90 (d, *J* = 8.7 Hz, 1H), 4.36 (s, 4H), 3.72 (s, 4H), 3.31 (s, 6H). ¹³C NMR (101 MHz, DMSO-*d*₆) δ 152.4, 151.8, 147.8, 131.8, 131.3, 106.0, 59.6, 50.3, 42.6.

The synthesis of compound 16

To a solution of **15** (920 mg, 3.74 mmol) in HCl (conc. 30 mL) was added HI (9.5 mL, 57%, w/w) dropwise at 0 °C. After the completion of the addition, the reaction mixture was warmed to room temperature and stirred for 1 h at room temperature. After that, a saturated aqueous solution of Na₂SO₃ (100 mL) was added, and the pH of the mixture was adjusted to 8 with an aqueous solution of 2 M NaOH. Then the solution was filtered through Celite and extracted with EtOAc (3 × 100 mL), and the obtained organic layer was dried over Na₂SO₄. After filtration and concentration, the obtained crude product was purified by chromatography on silica gel with ethyl acetate/petroleum ether (1/3, v/v) to give an orange solid product **16** (365 mg, 56%). ¹H NMR (400 MHz, DMSO-*d*₆) δ 7.44 (dd, *J* = 9.5, 5.9 Hz, 1H), 7.19 (s, 2H), 6.56 (t, *J* = 9.7 Hz, 1H), 5.20 (s, 2H).

The synthesis of compound 17

To a solution of **16** (55.5 mg, 0.32 mmol) in H₂O/AcOH (10/1, v/v, 4 mL) was added NaNO₂ (33.17 mg, 0.48 mmol) at room temperature. Then the reaction mixture was stirred for 1 h at room temperature. After completion of the reaction, the reaction mixture was extracted with EtOAc (3 × 30 mL), and the obtained organic phase was washed with 2 M HCl, saturated NaHCO₃ solution, and brine, successively. The organic phase was dried over Na₂SO₄. After filtration and concentration, the obtained crude product was purified by chromatography on silica gel with dichloromethane to give a yellow solid product **17** (56 mg, 95%). ¹H NMR (300 MHz, CDCl₃) δ 13.66 (s, 1H), 8.47 (d, *J* = 8.4 Hz, 1H), 7.22 (d, *J* = 8.6 Hz, 1H).

The synthesis of compound 8b

To a solution of **17** (25 mg, 0.14 mmol) in acetonitrile (2 mL) was added compound **11** (36.28 mg, 0.14 mmol) and triethylamine (27.78 mg, 0.27 mmol). The reaction mixture was stirred for 10 h at room temperature. After completion of the reaction, the reaction solution was filtered, and the filtrate was a yellow solid product. (40 mg, 68%). ¹H NMR (300 MHz, DMSO-*d*₆) δ 8.34 (d, *J* = 8.9 Hz, 1H), 6.91 (d, *J* = 9.3 Hz, 1H), 4.61 (s, 4H), 3.72 (s, 4H), 3.30 (s, 6H). ¹³C NMR (101 MHz, DMSO-*d*₆) δ 146.1, 135.4, 129.5, 126.9, 121.9, 104.8, 59.4, 50.2, 41.8.

The synthesis of compound 18

To a solution of 3'-chloro-acetanilid (600 mg, 2.95 mmol) in Ac₂O/AcOH (4/1, v/v, 5 mL) was added HNO₃ (445.82 mg, 5.90 mmol) dropwise at 0 °C. Then the reaction mixture was warmed to room temperature and stirred for another 5 h. After completion of the reaction, the reaction was quenched with H₂O (50 mL). Then the mixture was extracted with EtOAc (3 × 50 mL), and the obtained organic phase was washed with saturated NaHCO₃ solution until no bubbles were generated. The obtained organic phase was dried over Na₂SO₄. After filtration and concentration, the obtained crude product was purified by chromatography on silica gel with ethyl acetate/petroleum ether (1/5, v/v) to give a white solid product **18** (405 mg, 53%). ¹H NMR (300 MHz, DMSO-*d*₆) δ 10.43 (s, 1H), 8.90 (d, *J* = 2.0 Hz, 1H), 8.17 (d, *J* = 9.1 Hz, 1H), 7.14 (dd, *J* = 9.0, 2.1 Hz, 1H), 2.30 (s, 3H).

The synthesis of compound 19

To a solution of **18** (200 mg, 0.93 mmol) in methanol (5 mL) was added sodium methoxide (46.35 mg, 0.93 mmol), and the mixture was stirred for 2 h at room temperature. After completion of the reaction, the reaction was quenched with H₂O (30 mL) and extracted with EtOAc (3 × 30 mL). The obtained organic phase was dried over Na₂SO₄. After filtration and concentration, the obtained crude product was purified by chromatography on silica gel with petroleum ether/dichloromethane (1/1, v/v) to give a yellow solid product **19** (160 mg, 63%). ¹H NMR (300 MHz, DMSO-*d*₆) δ 7.98 (d, *J* = 9.2 Hz, 1H), 7.56 (s, 2H), 7.08 (s, 1H), 6.64 (d, *J* = 9.1 Hz, 1H).

The synthesis of compound 20

To a solution of **19** (200 mg, 1.16 mmol) and sodium hydroxide (46.35 mg, 1.16 mmol) in methanol (5 mL) was added sodium hypochlorite (4.31 g, 4%, w/w) at 0 °C. Then the reaction mixture was stirred for 1 h at 0 °C. After completion of the reaction, the reaction was quenched with H₂O (30 mL), and a yellow precipitate was formed, which was filtered, and redissolved in EtOAc (30 mL), and the solution was dried over Na₂SO₄. After filtration and concentration, the obtained crude product was purified by chromatography on silica gel with ethyl acetate/petroleum ether (1/20, v/v) to give a white solid product **20** (88 mg, 44%). ¹H NMR (300 MHz, DMSO-*d*₆) δ 8.06 (s, 1H), 7.81 (s, 1H), 7.48 (s, 1H).

The synthesis of compound 21

To a solution of **20** (50 mg, 0.29 mmol) in H₂SO₄ (3 mL) was added HNO₃ (55.42 mg, 0.44 mmol) dropwise at 0 °C. Then the reaction mixture was warmed to room temperature and stirred for another 0.5 h. After completion of the reaction, the reaction was quenched with H₂O (20 mL) and extracted with EtOAc (3 × 20 mL). The obtained organic phase was washed with saturated NaHCO₃ solution until no bubbles were generated and dried over Na₂SO₄. After filtration and concentration, the obtained crude product was purified by chromatography on silica gel with ethyl acetate/petroleum ether (1/5, v/v) to give a yellow solid product **21** (43 mg, 68%). ¹H NMR (300 MHz, CDCl₃) δ 7.60 (d, *J* = 9.8 Hz, 1H), 7.29 (d, *J* = 9.8 Hz, 1H).

General procedure B

To a solution of compound **21** (1.1 equiv.) in ACN/PBS (1/1, v/v, 3 mL) was added the nucleophile (1.0 equiv.). The obtained reaction mixture was stirred for 1–12 h at room temperature. After completion of the reaction, the reaction solution was filtered, and the filtrate was concentrated under reduced pressure. The obtained residue was purified by chromatography on silica gel or neutral alumina with methanol/dichloromethane to give the desired product.

The synthesis of compound 9a

Compound **9a** was synthesized according to the general procedure B as a dark red solid (20 mg, 32%). ¹H NMR (300 MHz, D₂O) δ 8.49 (d, *J* = 8.6 Hz, 1H), 6.64 (d, *J* = 8.6 Hz, 1H), 3.78 (s, 3H), 3.72 (d, *J* = 5.0 Hz, 4H), 3.29 (s, 6H). ¹³C NMR (101 MHz, DMSO-*d*₆) δ 147.7, 145.7, 136.4, 127.7, 112.9, 108.4, 60.3, 51.4, 45.1.

The synthesis of compound 9b

Compound **9b** was synthesized according to the general procedure B as a red solid (18 mg, 49%). ¹H NMR (300 MHz, CDCl₃) δ 8.33 (d, *J* = 8.4 Hz, 1H), 6.24 (d, *J* = 8.4 Hz, 1H), 3.40 (s, 4H), 3.12 (s, 4H).

The synthesis of compound 9c

Compound **9c** was synthesized according to the general procedure B as a red solid (20 mg, 38%). ¹H NMR (300 MHz, CDCl₃) δ 8.58 (s, 1H), 8.31 (d, *J* = 9.6 Hz, 1H), 7.28 (d, *J* = 11.3 Hz, 4H), 6.36 (d, *J* = 9.0 Hz, 1H), 2.42 (s, 3H).

The synthesis of compound 9e

Compound **9e** was synthesized according to the general procedure B as a red solid (20 mg, 56%). ^1H NMR (400 MHz, CDCl_3) δ 8.05 (d, J = 9.1 Hz, 1H), 5.99 (d, J = 9.2 Hz, 1H), 3.88 (m, J = 6.5 Hz, 4H), 1.37 (t, J = 7.0 Hz, 6H).

The synthesis of compound 9f

Compound **9f** was synthesized according to the general procedure B as a red solid (10 mg, 53%). ^1H NMR (300 MHz, CDCl_3) δ 8.17 (d, J = 8.8 Hz, 1H), 5.96 (d, J = 8.9 Hz, 1H), 2.26 (s, 4H), 1.35 (s, 4H).

The synthesis of compound 9d

To a solution of **9b** (20 mg, 0.08 mmol) in ACN/PBS (1/1, v/v, 2 mL) was added propyl chloroformate (13.86 mg, 0.11 mmol) and triethylamine (7.83 mg, 0.08 mmol), and the mixture was stirred for 1 h at room temperature. After completion of the reaction, the reaction mixture was poured into 20 mL water and was extracted with CH_2Cl_2 (3×20 mL). The obtained organic layer was then dried over Na_2SO_4 . After filtration and concentration, the obtained crude product was purified by chromatography on silica gel with methanol/dichloromethane to give a red solid product **9d** (10 mg, 38%). ^1H NMR (300 MHz, CDCl_3) δ 8.33 (d, J = 8.5 Hz, 1H), 6.28 (d, J = 8.6 Hz, 1H), 4.09 (t, J = 6.6 Hz, 2H), 3.78–3.68 (m, 4H), 3.37 (d, J = 4.8 Hz, 4H), 1.73–1.66 (m, 2H), 0.96 (t, J = 7.4 Hz, 3H).

The reaction between sulfonyl azide/7b and GSH

The reaction between sulfonyl azide **3/7b** and GSH was assayed in PBS (pH 7.4) at 37 °C using HPLC. Specifically, a solution of **3/7b** (100 μM) and GSH (1 mM) in 20% ACN/PBS was incubated at 37 °C, and an aliquot was taken at intervals for HPLC analysis. The results were summarized in Supplementary Figs. 10, and 11, and it can be seen that GSH can efficiently reduce sulfonyl azide **3** under such conditions, while no obvious adduct was formed between GSH and **7b**.

Biology

Instruments: Microplate Reader (Tecan, M1000 PRO), Shaker (Blue pard, THZ-100), Constant Temperature Incubator (Blue pard, DHP-9272), Automated Colony Counter (Shineso, Supcre G10), Ultracentrifuge (Eppendorf, 5404), CO_2 Incubator (Heal Force, HF151), Laser Product (CNI, MDL-HD-655). Bacterial strains and growth conditions: *Staphylococcus aureus* (*S. aureus* ATCC29213), *Pseudomonas aeruginosa* (*P. aeruginosa* 01), *Escherichia coli* (*E. coli* ATCC25922) and methicillin-resistant *Staphylococcus aureus* (MRSA ATCC43300) were grown in Mueller-Hinton Broth (MHB) without or with 200–500 μM L-cysteine and on LBA plates (LB supplemented with 1.5% Bacto agar) at 37 °C.

Animals and ethical statement

No permits were required for the study's sampling sites/activities following the regulations and guidelines of the Ethics Review Committee of Soochow University. Moreover, this study did not involve endangered or protected species. All animal testing protocols were conducted in compliance with Animal Welfare Act regulations and the 1996 National Research Council's Guide for Laboratory Animal Care and Use. Six- to eight-week-old female BALB/c mice (18–22 g) were purchased from the Chinese Academy of Military Medical Sciences (Beijing, China). Animals were housed on a 12-hour light-dark cycle. Room temperature was between 20–24 °C, and humidity was between 50–70%. The mice were fed the irradiated Teklad Global Rodent Diet and water ad libitum.

MB assay in the cell-free buffer

The H_2S -depletion ability of the tested compounds was evaluated with MB assay. Briefly, the tested compounds were dissolved in DMSO/PBS

(10%, pH 7.4) to prepare a 220 μM stock solution, which was mixed with a solution of Na_2S in a sealed flask (the final concentration of Na_2S and the tested compound was 100 μM and 110 μM , respectively). The Na_2S solution without the treatment of the test compounds was used as the control. The obtained solution was left at room temperature, and 100 μL of the solution was drawn off at intervals and added into a 96-well plate containing 100 μL of the methylene blue cocktail (20% of zinc acetate (1.00% w/v), 40% of FeCl_3 (30 mM in 1.20 M HCl) and 40% of *N,N*-dimethyl-*p*-phenylene diamine (20 mM in 7.20 M HCl)). After 30 min incubation at room temperature, the absorbance of the samples at 676 nm was recorded using a microplate reader, and the concentration of H_2S in each well was calculated using the calibration curve of H_2S . The obtained H_2S concentrations were plotted against the time, and the H_2S decay half-life can be calculated accordingly. The experiment was replicated, and the results were expressed as mean \pm SD (n = 3 independent experiments). Some of the results are summarized in Supplementary Fig. 14.

MB assay in bacterial cells

The H_2S -depletion capacity of the tested compounds in bacteria was also assayed with the MB assay. Specifically, overnight cultures were inoculated into MHB supplemented with 0.5 mM L-cysteine and grown at 37 °C to 4×10^8 CFU/mL. The tested compounds were dissolved in 1% of DMSO/PBS and added to the bacteria (The final concentration of bacteria was 2×10^8 CFU/mL, and the concentrations of the tested compounds were 100, 50, 25, 12.5, 6.5, 3.125 μM). Then the bacteria suspensions were incubated at 37 °C for 12 h. The samples were centrifuged at $6026 \times g$, 4 °C for 5 min, and 100 μL of the supernatant was taken and added into a 96-well plate containing 100 μL of the MB cocktail. After 30 min incubation at room temperature, the absorbance of the samples at 676 nm was recorded using a microplate reader, and the concentration of H_2S was calculated using the calibration curve. The experiment was replicated, and the results are expressed as mean \pm SD (n = 3 biological replicates). The results are summarized in Supplementary Figs. 15, 16.

Lead acetate paper strip assay

The H_2S -depletion activity of the tested compounds in bacteria was evaluated by the lead acetate paper strip assay. Specifically, overnight cultures were grown to 4×10^8 CFU/mL in MHB without or with L-cysteine (500 μM). Then different concentrations of H_2S scavengers were added to the bacteria. (The final concentration of bacteria was 2×10^8 CFU/mL, and the concentrations of the scavengers were 100, 50, 25, 12.5, 6.5, and 3.125 μM). The paper strips saturated by 2% Pb-acetate were affixed to the inner wall of a 4 mL cultural tube above the level of the liquid culture of the samples. The tubes containing the bacteria suspensions were incubated at 37 °C for 12 h. Stained paper strips of bacterial suspensions were compared and a darker color of the paper indicates more H_2S was in the samples.

Antibiotic MIC determination

All strains used in this research are listed in Supplementary Table 1. The standard strains were sourced from the American Type Culture Collection (ATCC). The gene-knockout strain was generously provided by Professor Yongzhen Xia from Shandong University. Overnight cultures were grown to 1×10^8 CFU/mL in MHB and diluted with MHB to 2×10^5 CFU/mL. A serial dilution of antibiotics was prepared in 96-well microtiter plates and mixed with equal volumes of diluted bacteria. The plates were incubated at 37 °C for 16 h with a shaking speed of 110 rpm. After incubation, the absorbance at 600 nm of the bacteria suspensions was recorded using a microplate reader. The minimal concentrations at which no microbial growth occurred were recorded as MIC (minimal inhibitory concentration) values. The results were summarized in Supplementary Table 1.

Time-dependent killing assay

The bacterial survival curves with or without antibiotics were generated by the LB agar plating method. Specifically, overnight cultures were inoculated into MHB supplemented with 0.5 mM Cys and grown at 37 °C to 1×10^8 CFU/mL and diluted with 0.9% NaCl to 5×10^5 CFU/mL. Then, the tested compounds (antibiotics, H₂S scavengers, Na₂S, or different combinations) were added to the diluted bacteria solution. Then, the samples were incubated at 37 °C and were diluted 1000 times at different time points (0, 0.5, 1, 2 h, or 0, 2, 4 and 6 h). The diluted samples were placed on LB agar and incubated at 37 °C for 16 h. Cell survival was determined by counting CFU and was shown as the mean \pm SD from three independent experiments.

Mammalian cell cytotoxicity assay

The HEK 293 cells were purchased from the Cell Bank of the Chinese Academy of Sciences (Shanghai, China). HEK 293 cells were cultured in high glucose DMEM medium with 10% fetal bovine serum and 1% penicillin/streptomycin under standard cell culture conditions at 37 °C in a humidified incubator with 5% CO₂. The cytotoxicity of **7b** in combination with different antibiotics was determined via a Cell Counting Kit-8 (CCK-8) assay in the HEK 293 cells. Briefly, the cells were seeded to the 96-well plate at a density of 8000/well and were cultured overnight before experiments. After that, the culture medium was replaced with a fresh one containing **7b** (0–200 μ M), different antibiotics (gentamicin, vancomycin, ciprofloxacin, erythromycin, or ampicillin), or both for 24 h. Then, the old medium was discarded, and 10% CCK8 medium was added to each well. The samples were incubated for another 1–2 h, and the absorbance of the samples at 450 nm was recorded using a microplate reader. The results were summarized in Supplementary Fig. 24.

Biofilm inhibition assay

Biofilm inhibition assay was performed in a 96-well plate using the crystal violet staining method. Briefly, overnight cultures were inoculated into MHB supplemented with 0.5 mM Cys and were diluted with MHB to 2×10^7 CFU/mL. The diluted bacteria were distributed to a 96-well plate. Different concentrations of the H₂S scavenger **7b** (25, 12.5, 6.25 μ M) were added into each well with or without 200 μ M of Na₂S. The bacteria suspensions were incubated at 37 °C for 24 h. Then, planktonic cells were removed, and wells were washed with PBS three times. 100 μ L crystal violet solution (0.1%, v/v) was then added and incubated at 37 °C for another 15 min. After that, the crystal violet solution was removed, and the wells were washed with PBS 3 times. 100 μ L of ethanol (30%, v/v) was added to each well and incubated at 37 °C for 30 min. Then the absorbance of the samples at 595 nm was recorded using a microplate reader. The experiment was replicated, and the results are expressed as mean \pm SD ($n = 3$ biological replicates).

Biofilm eradication assay

Briefly, overnight cultures were inoculated into MHB supplemented with 0.5 mM Cys and were diluted with MHB to 1×10^7 CFU/mL. The diluted bacteria were distributed to a 96-well plate and incubated at 37 °C for 24 h. Then, planktonic cells were removed, and wells were washed with PBS 3 times. Different concentrations of the H₂S scavenger **7b** (25, 12.5, 6.25 μ M) were added into each well with or without 200 μ M of Na₂S. And the incubation was continued at 37 °C for 24 h. Then, planktonic cells were removed, and wells were washed with PBS three times. 100 μ L crystal violet solution (0.1%, v/v) was added to each well and incubated at 37 °C for 15 min. Then, the crystal violet solution was removed, and the wells were washed with PBS 3 times. Afterward, 100 μ L of ethanol (30%, v/v) was added to each well and incubated at 37 °C for 30 min. Then the absorbance of the samples at 595 nm was recorded using a microplate reader. The experiment was replicated, and the results are expressed as mean \pm SD ($n = 3$ biological replicates).

Persister cells eradication assay

Persister cells eradication assay was conducted with the LB agar plating method. Briefly, overnight cultures were inoculated into MHB supplemented with 0.5 mM Cys and were diluted with MHB to 5×10^7 CFU/mL. The diluted bacteria were distributed in antibiotics at a concentration of $10 \times$ MIC ($20 \times$ MIC for *P. aeruginosa*) for 18 h. All of the bacteria were washed to remove antibiotics. The control bacteria were treated with the same concentration of antibiotics, and the experimental group was co-treated with **7b** and antibiotics. The incubation was continued at 37 °C. At variable time points, both bacteria suspensions were individually sampled, and the samples were subjected to serial dilution in PBS and checking of CFU from incubation on agar plates. The surviving bacteria were determined by counting CFU. The experiment was replicated, and the results are expressed as mean \pm SD ($n = 3$ biological replicates).

Antibacterial activity of photosensitizer combined with compound 7b

The antibacterial activity of photosensitizer (**Ce6**) combined with H₂S scavengers **7b** was evaluated by the LB agar plating method. Specifically, overnight cultures were inoculated into MHB supplemented with 0.5 mM Cys and grown at 37 °C to 5×10^8 CFU/mL. Then, cells were diluted 100 times in sterile 0.9% NaCl and treated with **Ce6** (concentrations used for *S. aureus*, *P. aeruginosa*, *E. coli*, and MRSA were 1, 20, 10, and 10 μ M, respectively), or **Ce6** + **7b** (25 μ M) at room temperature in the dark for 5 min. The samples were then irradiated under 665 nm light (0.1 mW cm⁻² for *S. aureus*, 1 mW cm⁻² for *P. aeruginosa*, *E. coli*, and MRSA) for the different periods (40 s for *S. aureus*, 3 min for *P. aeruginosa*, 1.5 min for *E. coli*, and 1 min for MRSA). Then the samples were diluted 100 times and placed on an LB agar plate, and incubated at 37 °C for 16 h. The samples kept in the dark were used as controls. The surviving bacteria were determined by counting CFU. The experiment was replicated, and the results are expressed as mean \pm SD ($n = 3$ biological replicates).

Phagocytosis of macrophages assay

RAW 264.7 cells were purchased from the Cell Bank of the Chinese Academy of Sciences (Shanghai, China), and were cultured in high glucose DMEM medium with 10% fetal bovine serum and 1% penicillin/streptomycin under standard cell culture conditions at 37 °C in a humidified incubator with 5% CO₂. *S. aureus*, *E. coli* or PAOI was opsonized by incubation with 10% mouse serum at room temperature for 30 min and then incubated at 37 °C with high glucose DMEM medium with 10% fetal bovine serum (FBS) at a multiplicity of infection (MOI) of 5:1 for 1 h. Briefly, 1×10^5 RAW 264.7 cells were seeded onto 48-well plates and allowed to adhere overnight. The planktonic cells were removed with PBS washing, and the bacteria were then added at an MOI of 5:1. The plates were then incubated at 37 °C for 1 h. To enumerate viable intracellular bacteria, cells were washed twice with PBS after 1 h of incubation with bacteria and were treated with 100 μ g/mL gentamicin for 30 min to kill extracellular bacteria. Then the plates were washed twice with PBS and were incubated with H₂S scavenger **7b**. After 0.5, 1, and 2 h of incubation, cells were washed twice with PBS and lysed with 1 mL 0.03% Triton X-100. Then 50 μ L of the lysed solution was placed on an LB agar and incubated at 37 °C for 16 h. The surviving bacteria were determined by counting CFU. The experiment was replicated, and the results are expressed as mean \pm SD ($n = 3$ biological replicates).

Production of TNF- α in Macrophages

RAW264.7 cells were seeded at a density of 2×10^6 cells per well in 6-well plates and cultured overnight in DMEM supplemented with 10% FBS. Before infection, the wild-type *P. aeruginosa* was preconditioned in DMEM for 30 minutes. Following two rounds of PBS washing of the RAW264.7 cells, 500 μ L of DMEM containing 4×10^7 CFU/mL of *P. aeruginosa* was added to achieve a multiplicity of infection (MOI) of 10.

Subsequently, compound **7b** was introduced to the wells with a final concentration of 25 μ M. After two hours of incubation, the cell supernatant was collected for analysis. The concentration of TNF- α in the supernatant was determined using a TNF- α assay kit from Invitrogen to quantify the cytokine levels.

Phagocytosis of neutrophils assay

Neutrophils from the bone marrow of femurs and tibiae in 10-week-old mice were segregated using a tripartite Percoll gradient of 78, 69, and 52%. The bacterial phagocytosis assay was performed following Kasorn's protocol⁶⁴. Specifically, *P. aeruginosa* was cultured at 37 °C overnight to reach its logarithmic phase of growth, followed by a pre-treatment phase in RPMI-1640 medium enriched with 10% mouse serum for 30 minutes at the same temperature. To attain an MOI of 5×10^5 CFU of these pre-treated bacteria were then added to 1×10^5 neutrophils in the presence/absence of 25 μ M of the compound **7b**. Both experimental and control setups underwent incubation at 37 °C for 2 h. Neutrophils were subsequently lysed using 1% Triton-X. Enumeration of the surviving bacteria was performed by plating triplicate serial dilutions on LB agar plates. The survival rate of bacteria was assessed by comparing the CFU with those from identical experimental setups involving untreated bacteria (absent neutrophils), ensuring consistent experimental conditions and distribution on plates. Neutrophil-mediated bacterial killing rate (%) = $(N^0 - N) / N^0 \times 100\%$, wherein N^0 represents the count of bacterial colonies observed when neutrophils are absent at a given time point, whereas N denotes the colony counts within the treatment group.

Murine lung infection model

All animal experiment protocols were approved by the Animal Care and Use Committee of Soochow University and complied with all relevant ethical regulations.

Six- to eight-week-old female BALB/c mice (18–22 g) were purchased from the Chinese Academy of Military Medical Sciences (Beijing, China). The animals were acclimated for at least 24 hours before the experiment. The mice were fed the irradiated Teklad Global Rodent Diet and water ad libitum. Eight mice in each group were allocated to two static cages.

P. aeruginosa (both wild-type and mutant strains) was grown in 5 mL of MHB at 37 °C in an ambient atmosphere overnight. Then cultures were centrifuged at $6026 \times g$ at 25 °C for 5 min. The pellet was resuspended in 5 mL of PBS, centrifuged, and resuspended in 5 mL of PBS. The procedure was repeated 3 times. Then the resuspended solution was diluted to 1×10^7 CFU/mL with PBS. Mice were flash anesthetized with isoflurane gas and infected intranasally with 5×10^5 CFU/mouse of bacteria in 50 μ L. At 30 min after infection, gentamicin and **7b** were administered by subcutaneous (s.c.) route at 10 mL/kg. Group 1: 10% DMSO/PBS ($n = 8$); Group 2: Gentamicin (20 mg/kg) ($n = 8$); Group 3: Gentamicin (20 mg/kg) + **7b** (20 mg/kg) ($n = 8$); Group 4: **7b** (20 mg/kg) ($n = 8$).

After 24 h of drug administration, the mice were sacrificed, and the thoracic cavity of the mice was cut open with a scalpel. Lungs of mice were cannulated via the trachea and lavaged with a volume of 1 mL of PBS. Meanwhile, the lung of the mice was harvested and ground into liquid by a homogenizer. The resultant homogenate and Bronchoalveolar Lavage Fluid (BALF) was serially diluted (The PBS and **7b** group was diluted 1,000,000 times; The Gm group was diluted 10,000 times; The Gm + **7b** group was diluted 1000 times). The organ homogenate and BALF samples were inoculated onto LB agar plates and incubated at 37 °C for 16 h. The bacterial load can be quantified by utilizing an automated colony counting apparatus (Supcre G10, Shineso Technology, Hangzhou) to enumerate CFUs, and the results are summarized in Supplementary Fig. 26.

The skin wound infection mouse model

Six- to eight-week-old female BALB/c mice (18–22 g) were purchased from the Chinese Academy of Military Medical Sciences (Beijing, China). The animals were housed on a 12-hour light-dark cycle. Room temperature was between 20–24 °C, and humidity was between 50–70%. The mice were fed the irradiated Teklad Global Rodent Diet and water ad libitum. All animal experiment protocols were approved by the Animal Care and Use Committee of Soochow University and complied with all relevant ethical regulations.

Our study included 13 mice per group, divided into two subsets: 5 for monitoring wound healing and 8 for evaluating bacterial colonization in the wounds. In brief, symmetrical circular wounds, each 1 cm in diameter, were created on the dorsal surface of the mice. Subsequently, 50 μ L of a bacterial suspension (5×10^8 CFU/mL) was injected into each wound. At 24, 48, and 72 h after infection, the mice received different treatments through the injection of PBS, gentamicin (1 mg/kg), **7b** (20 mg/kg), or a combination of gentamicin (1 mg/kg) and compound **7b** (20 mg/kg) directly into the wound area, respectively. Wound healing was observed at predetermined times after infection, and on the fourth day post-infection, the wound areas were homogenized to evaluate bacterial colonization. The representative pictures of the wound areas in different treatment groups were summarized in Supplementary Fig. 27.

Reporting summary

Further information on research design is available in the Nature Portfolio Reporting Summary linked to this article.

Data availability

All data generated and/or analyzed in this study are provided in the paper or are appended as supplementary data. Source data are provided in this paper.

References

- Murray, C. J. L. et al. Global burden of bacterial antimicrobial resistance in 2019: a systematic analysis. *Lancet* **399**, 629–655 (2022).
- Brown, E. D. & Wright, G. D. Antibacterial drug discovery in the resistance era. *Nature* **529**, 336–343 (2016).
- Blair, J. M. A., Webber, M. A., Baylay, A. J., Ogbolu, D. O. & Piddock, L. J. V. Molecular mechanisms of antibiotic resistance. *Nat. Rev. Microbiol.* **13**, 42–51 (2015).
- Mitcheltree, M. J. et al. A synthetic antibiotic class overcoming bacterial multidrug resistance. *Nature* **599**, 507–512 (2021).
- Durand-Reville, T. F. et al. Rational design of a new antibiotic class for drug-resistant infections. *Nature* **597**, 698–702 (2021).
- Imai, Y. et al. A new antibiotic selectively kills Gram-negative pathogens. *Nature* **576**, 459–464 (2019).
- Smith, P. A. et al. Optimized arylomycins are a new class of Gram-negative antibiotics. *Nature* **561**, 189–194 (2018).
- Durand-Reville, T. F. et al. ETX2514 is a broad-spectrum β -lactamase inhibitor for the treatment of drug-resistant Gram-negative bacteria including *Acinetobacter baumannii*. *Nat. Microbiol.* **2**, 17104 (2017).
- Wang, Z. et al. A naturally inspired antibiotic to target multidrug-resistant pathogens. *Nature* **601**, 606–611 (2022).
- Li, Q. et al. Synthetic group A streptogramin antibiotics that overcome Van resistance. *Nature* **586**, 145–150 (2020).
- Stokes, J. M. et al. Pentamidine sensitizes Gram-negative pathogens to antibiotics and overcomes acquired colistin resistance. *Nat. Microbiol.* **2**, 17028 (2017).
- King, A. M. et al. Aspergillomarasmine A overcomes metallo- β -lactamase antibiotic resistance. *Nature* **510**, 503–506 (2014).
- Song, M. et al. A broad-spectrum antibiotic adjuvant reverses multidrug-resistant Gram-negative pathogens. *Nat. Microbiol.* **5**, 1040–1050 (2020).

14. Yu, B. et al. Restoring and enhancing the potency of existing antibiotics against drug-resistant gram-negative bacteria through the development of potent small-molecule adjuvants. *ACS Infect. Dis.* **8**, 1491–1508 (2022).
15. Douafer, H., Andrieu, V., Phanstiel, O. & Brunel, J. M. Antibiotic adjuvants: Make antibiotics great again! *J. Med. Chem.* **62**, 8665–8681 (2019).
16. Zhu, Y. et al. Antimicrobial peptides, conventional antibiotics, and their synergistic utility for the treatment of drug-resistant infections. *Med. Res. Rev.* **42**, 1377–1422 (2022).
17. Parker, E. N. et al. An iterative approach guides discovery of the FabI inhibitor fabimycin, a late-stage antibiotic candidate with in vivo efficacy against drug-resistant gram-negative infections. *ACS Cent. Sci.* **8**, 1145–1158 (2022).
18. Parker, E. N. et al. Implementation of permeation rules leads to a FabI inhibitor with activity against Gram-negative pathogens. *Nat. Microbiol.* **5**, 67–75 (2020).
19. Ni, N., Li, M., Wang, J. & Wang, B. Inhibitors and antagonists of bacterial quorum sensing. *Med. Res. Rev.* **29**, 65–124 (2009).
20. Whiteley, M., Diggle, S. P. & Greenberg, E. P. Progress in and promise of bacterial quorum sensing research. *Nature* **551**, 313–320 (2017).
21. Corona, F. & Martinez, J. L. Phenotypic resistance to antibiotics. *Antibiotics* **2**, 237–255 (2013).
22. Keren, I., Kaldalu, N., Spoering, A., Wang, Y. & Lewis, K. Persister cells and tolerance to antimicrobials. *FEMS Microbiol. Lett.* **230**, 13–18 (2004).
23. Fauvart, M., De Groote, V. N. & Michiels, J. Role of persister cells in chronic infections: clinical relevance and perspectives on anti-persister therapies. *J. Med. Microbiol.* **60**, 699–709 (2011).
24. Levin-Reisman, I. et al. Antibiotic tolerance facilitates the evolution of resistance. *Science* **355**, 826–830 (2017).
25. Fridman, O., Goldberg, A., Ronin, I., Shosh, N. & Balaban, N. Q. Optimization of lag time underlies antibiotic tolerance in evolved bacterial populations. *Nature* **513**, 418–421 (2014).
26. Schrader, S. M., Vaubourgeix, J. & Nathan, C. Biology of anti-microbial resistance and approaches to combat it. *Sci. Transl. Med.* **12**, eaaz6992 (2020).
27. Kim, W. et al. A new class of synthetic retinoid antibiotics effective against bacterial persisters. *Nature* **556**, 103–107 (2018).
28. Kaldalu, N. et al. In vitro studies of persister cells. *Microbiol. Mol. Biol. Rev.* **84**, e00070–20 (2020).
29. Hartle, M. D. & Pluth, M. D. A practical guide to working with H₂S at the interface of chemistry and biology. *Chem. Soc. Rev.* **45**, 6108–6117 (2016).
30. Shatalin, K., Shatalina, E., Mironov, A. & Nudler, E. H₂S: a universal defense against antibiotics in bacteria. *Science* **334**, 986–990 (2011).
31. Shatalin, K. et al. Inhibitors of bacterial H₂S biogenesis targeting antibiotic resistance and tolerance. *Science* **372**, 1169–1175 (2021).
32. Cao, X. et al. A review of hydrogen sulfide synthesis, metabolism, and measurement: Is modulation of hydrogen sulfide a novel therapeutic for cancer? *Antioxid. Redox Signal.* **31**, 1–38 (2019).
33. Ma, Y. et al. CBS-derived H₂S facilitates host colonization of *Vibrio cholerae* by promoting the iron-dependent catalase activity of KatB. *PLoS Path.* **17**, e1009763 (2021).
34. Yang, J. et al. Non-enzymatic hydrogen sulfide production from cysteine in blood is catalyzed by iron and vitamin B6. *Commun. Biol.* **2**, 194 (2019).
35. Moest, R. R. Hydrogen sulfide determination by the methylene blue method. *Anal. Chem.* **47**, 1204–1205 (1975).
36. Jiang, C. et al. NBD-based synthetic probes for sensing small molecules and proteins: design, sensing mechanisms and biological applications. *Chem. Soc. Rev.* **50**, 7436–7495 (2021).
37. Yang, C.-T. et al. Data-driven identification of hydrogen sulfide scavengers. *Angew. Chem. Int. Ed.* **58**, 10898–10902 (2019).
38. Lin, V. S. & Chang, C. J. Fluorescent probes for sensing and imaging biological hydrogen sulfide. *Curr. Opin. Chem. Biol.* **16**, 595–601 (2012).
39. Lin, V. S., Chen, W., Xian, M. & Chang, C. J. Chemical probes for molecular imaging and detection of hydrogen sulfide and reactive sulfur species in biological systems. *Chem. Soc. Rev.* **44**, 4596–4618 (2015).
40. Peng, H. et al. A fluorescent probe for fast and quantitative detection of hydrogen sulfide in blood. *Angew. Chem. Int. Ed.* **50**, 9672–9675 (2011).
41. Fiorot, R. G., de, M. & Carneiro, J. W. The mechanism for H₂S scavenging by 1,3,5-hexahydrotriazines explored by DFT. *Tetrahedron* **76**, 131112 (2020).
42. Henthorn, H. A. & Pluth, M. D. Mechanistic insights into the H₂S-mediated reduction of aryl azides commonly used in H₂S detection. *J. Am. Chem. Soc.* **137**, 15330–15336 (2015).
43. Ismail, I. et al. Highly efficient H₂S scavengers via thiolysis of positively-charged NBD amines. *Chem. Sci.* **11**, 7823–7828 (2020).
44. Xia, Y. et al. Sulfide production and oxidation by heterotrophic bacteria under aerobic conditions. *ISME J.* **11**, 2754–2766 (2017).
45. Hammers, M. D. & Pluth, M. D. Ratiometric measurement of hydrogen sulfide and cysteine/homocysteine ratios using a dual-fluorophore fragmentation strategy. *Anal. Chem.* **86**, 7135–7140 (2014).
46. Montoya, L. A., Pearce, T. F., Hansen, R. J., Zakharov, L. N. & Pluth, M. D. Development of selective colorimetric probes for hydrogen sulfide based on nucleophilic aromatic substitution. *J. Org. Chem.* **78**, 6550–6557 (2013).
47. Mironov, A. et al. Mechanism of H₂S-mediated protection against oxidative stress in *Escherichia coli*. *Proc. Natl. Acad. Sci. USA* **114**, 6022–6027 (2017).
48. Shukla, P. et al. On demand” redox buffering by H₂S contributes to antibiotic resistance revealed by a bacteria-specific H₂S donor. *Chem. Sci.* **8**, 4967–4972 (2017).
49. Zheng, Y. et al. Toward hydrogen sulfide based therapeutics: Critical drug delivery and developability issues. *Med. Res. Rev.* **38**, 57–100 (2018).
50. Toliver-Kinsky, T. et al. H₂S, a Bacterial defense mechanism against the host immune response. *Infect. Immun.* **87**, e00272–00218 (2019).
51. Forte, E. et al. The terminal oxidase cytochrome bd promotes sulfide-resistant bacterial respiration and growth. *Sci. Rep.* **6**, 23788 (2016).
52. Thees, A. V. et al. PmtA regulates pyocyanin expression and biofilm formation in *Pseudomonas aeruginosa*. *Front. Microbiol.* **12**, 789765 (2021).
53. Okshevsky, M. & Meyer, R. L. The role of extracellular DNA in the establishment, maintenance and perpetuation of bacterial biofilms. *Crit. Rev. Microbiol.* **41**, 341–352 (2015).
54. Ronneau, S., Hill, P. W. & Helaine, S. Antibiotic persistence and tolerance: not just one and the same. *Curr. Opin. Microbiol.* **64**, 76–81 (2021).
55. Dilek, N., Papapetropoulos, A., Toliver-Kinsky, T. & Szabo, C. Hydrogen sulfide: An endogenous regulator of the immune system. *Pharmacol. Res.* **161**, 105119 (2020).
56. Miao, L., Xin, X., Xin, H., Shen, X. & Zhu, Y. Z. Hydrogen sulfide recruits macrophage migration by integrin β 1-Src-FAK/Pyk2-Rac pathway in myocardial infarction. *Sci. Rep.* **6**, 22363 (2016).
57. Keren, I., Wu, Y., Inocencio, J., Mulcahy, L. R. & Lewis, K. Killing by bactericidal antibiotics does not depend on reactive oxygen species. *Science* **339**, 1213–1216 (2013).
58. Szabo, C. Gasotransmitters in cancer: from pathophysiology to experimental therapy. *Nat. Rev. Drug Discov.* **15**, 185–203 (2016).
59. Ono, K. et al. Cysteine hydropersulfide inactivates β -lactam antibiotics with formation of ring-opened carbothioic S-acids in bacteria. *ACS Chem. Biol.* **16**, 731–739 (2021).

60. Walsh, B. J. C. et al. The response of *acinetobacter baumannii* to hydrogen sulfide reveals two independent persulfide-sensing systems and a connection to biofilm regulation. *mBio* **11**, <https://doi.org/10.1128/mbio.01254-20> (2020).
61. Fu, L. H. et al. Hydrogen sulfide inhibits the growth of *Escherichia coli* through oxidative damage. *J. Microbiol.* **56**, 238–245 (2018).
62. Ooi, X. J. & Tan, K. S. Reduced glutathione mediates resistance to H₂S toxicity in oral streptococci. *Appl. Environ. Microbiol.* **82**, 2078–2085 (2016).
63. Ng, S. Y. et al. Hydrogen sulfide sensitizes *acinetobacter baumannii* to killing by antibiotics. *Front. Microbiol.* **11**, 1875 (2020).
64. Kasorn, A. et al. Focal adhesion kinase regulates pathogen-killing capability and life span of neutrophils via mediating both adhesion-dependent and -independent cellular signals. *J. Immunol.* **183**, 1032–1043 (2009).

Acknowledgements

The wild type and the *cbs/cse* knockout strain of *P. aeruginosa* are generous gifts from Dr. Yongzhen Xia at Shandong University. This work was financially supported by the National Natural Science Foundation of China (22277087 to X.J., 32070439 to Y.W., U2106227 to W.Z. and 82022066 to W.Z.), Jiangsu Specially-Appointed Professor Program, the Key Research & Development Plan in Social Development of Jiangsu Province (BE2022723 to Y.W.), Suzhou Agricultural Science and Technology Innovation Project (SNG2022054 to Y.W.), and the Priority Academic Program Development of the Jiangsu Higher Education Institutes (PAPD).

Author contributions

X.J. and Y.W. conceived and supervised the project. J.S. and Y.G. conducted the chemical synthesis and in vitro antibacterial activity test. Xu W. and S.L. conducted all the animal experiments. Y.H. conducted the HPLC analysis. Z.H., Xia W., and M.L. assisted with both in vivo and in vitro antibacterial assays. B.F., W.Z., and C.Q. helped with the data analysis and provided conceptual advice. All authors reviewed and commented on the manuscript and approved its final submission.

Competing interests

The authors declare no competing interests.

Additional information

Supplementary information The online version contains supplementary material available at <https://doi.org/10.1038/s41467-024-53764-7>.

Correspondence and requests for materials should be addressed to Wei Zhang, Yipeng Wang or Xingyue Ji.

Peer review information *Nature Communications* thanks David Giedroc, and the other anonymous reviewers for their contribution to the peer review of this work. A peer review file is available.

Reprints and permissions information is available at <http://www.nature.com/reprints>

Publisher's note Springer Nature remains neutral with regard to jurisdictional claims in published maps and institutional affiliations.

Open Access This article is licensed under a Creative Commons Attribution-NonCommercial-NoDerivatives 4.0 International License, which permits any non-commercial use, sharing, distribution and reproduction in any medium or format, as long as you give appropriate credit to the original author(s) and the source, provide a link to the Creative Commons licence, and indicate if you modified the licensed material. You do not have permission under this licence to share adapted material derived from this article or parts of it. The images or other third party material in this article are included in the article's Creative Commons licence, unless indicated otherwise in a credit line to the material. If material is not included in the article's Creative Commons licence and your intended use is not permitted by statutory regulation or exceeds the permitted use, you will need to obtain permission directly from the copyright holder. To view a copy of this licence, visit <http://creativecommons.org/licenses/by-nc-nd/4.0/>.

© The Author(s) 2024